symmetry

MDPI

Review

The Scale-Invariant Vacuum Paradigm: Main Results and Current Progress Review (Part II) †

Vesselin G. Gueorguiev [1,2,*] and Andre Maeder [3]

[1] Institute for Advanced Physical Studies, 1784 Sofia, Bulgaria
[2] Ronin Institute for Independent Scholarship, 127 Haddon Pl., Montclair, NJ 07043, USA
[3] Geneva Observatory, University of Geneva, Chemin des Maillettes 51, CH-1290 Sauverny, Switzerland; andre.maeder@unige.ch
* Correspondence: vesselin@mailaps.org

† While the present paper is very much influenced buy our previous paper in *Universe* **2022**, *8*, 213, its extra labeling by (Part II) refers to its original intend to be a sequel to the paper "Action Principle for Scale Invariance and Applications (Part I)" published as *Symmetry* **2023**, *15*, 1966.

Abstract: This is a summary of the main results within the Scale-Invariant Vacuum (SIV) paradigm based on Weyl integrable geometry. We also review the mathematical framework and utilize alternative derivations of the key equations based on the reparametrization invariance as well. The main results discussed are related to the early universe; that is, applications to inflation, Big Bang Nucleosynthesis, and the growth of the density fluctuations within the SIV. Some of the key SIV results for the early universe are a natural exit from inflation within the SIV in a later time $t_{\rm exit}$ with value related to the parameters of the inflationary potential along with the possibility for the density fluctuations to grow sufficiently fast within the SIV without the need for dark matter to seed the growth of structure in the universe. In the late-time universe, the applications of the SIV paradigm are related to scale-invariant dynamics of galaxies, MOND, dark matter, and dwarf spheroidals, where one can find MOND to be a peculiar case of the SIV theory. Finally, within the recent time epoch, we highlight that some of the change in the length-of-the-day (LOD), about 0.92 cm/yr, can be accounted for by SIV effects in the Earth–Moon system.

Keywords: cosmology: theory, dark matter, dark energy, inflation; galaxies: formation, rotation; Weyl integrable geometry; Dirac co-calculus

check for updates

Citation: Gueorguiev, V.G.; Maeder, A. The Scale-Invariant Vacuum Paradigm: Main Results and Current Progress Review (Part II). *Symmetry* **2024**, *16*, 657. https://doi.org/10.3390/sym16060657

Academic Editor: Eduardo Guendelman

Received: 24 April 2024
Revised: 16 May 2024
Accepted: 23 May 2024
Published: 26 May 2024

Copyright: © 2024 by the authors. Licensee MDPI, Basel, Switzerland. This article is an open access article distributed under the terms and conditions of the Creative Commons Attribution (CC BY) license (https://creativecommons.org/licenses/by/4.0/).

1. Motivation

The paper is a summary of the main results, as of mid-year 2023, within the Scale-Invariant Vacuum (SIV) paradigm as related to Weyl integrable geometry (WIG) as an extension to the standard Einstein general relativity (EGR). Our main goal is to present a condensed overview of the key results of the theory so far, along with the latest progress in applying the SIV paradigm to variety of physics phenomena, and, in doing so, to help the intellectually curious reader gain some understanding as to where the paradigm has been tested and what is the success level of the inquiry. As such, the paper follows closely our previous 2022 paper Gueorguiev and Maeder [1] that was based on the talk presented at the conference Alternative Gravities and Fundamental Cosmology, at the University of Szczecin, Poland in September 2021. Our initial presentation and its conference contribution covered, back then, only four main results: comparing the scale factor $a(t)$ within ΛCDM and the SIV [2], the growth of the density fluctuations within the SIV [3], the application to scale-invariant dynamics of galaxies [4], and inflation of the early universe within the SIV theory [5]. Back then, our article layout aimed to focus on each of these four main results by highlighting its most relevant figure or equation. As a result, each topic was covered via one to two pages text preceded by short and concise description of the mathematical framework.

Here, we add a few new sections, one on the possible differentiators of the SIV from ΛCDM based on our earlier paper [6], with a specific emphasis on the distance moduli as function of the redshift, along with three new topic sections related to the recent developments in the application of the SIV paradigm since our previous summary paper in 2022 [1]. The sections are about MOND as a peculiar case of the SIV theory [4], local dynamical effects within the SIV as pertained to the lunar recession [7], and our latest study of the Big Bang Nucleosynthesis (BBNS) within the SIV paradigm [8], along with an Appendix A on the error by Banik and Kroupa concerning the Lunar Motion in the SIV theory. While the present paper is very much influenced by our previous 2022 paper [1], as noted in the title note above, its extra labeling of (Part II) refers to its original intent to be a sequel to the paper "Action Principle for Scale Invariance and Applications (Part I)" published in the first part of the special issue "Nature and Origin of Dark Matter and Dark Energy" [9].

The paper commences with this brief motivation section as an overview of scale invariance in relation to physical reality, along with a comparison of Einstein's general relativity and Weyl integrable geometry. In Section 2.1, we present a concise review of the mathematical framework encompassing Weyl integrable geometry, Dirac co-calculus, and reparametrization invariance. Instead of re-deriving the weak-field SIV results [9], the concept of reparametrization invariance [10] is employed to illustrate the corresponding equations of motion. The relevant discussion on reparametrization invariance is provided in Section 2.2, which addresses the implications of venturing beyond Einstein's general relativity. Section 2.3 presents a summary of the essential concepts of the scale-invariant cosmology, which are crucial for understanding the Section on comparisons and applications. In Section 3, the primary findings related to the early and late universe are presented in the order outlined in the table of contents and discussed at the beginning of this section. The paper concludes with Section 4 containing the conclusions and outlook for potential directions for future research.

1.1. Scale Invariance and Physical Reality

The existence of a scale is related to the presence of physical connection and causality. The corresponding relationships are formulated as physical laws expressed in mathematical equations. Numerical factors in the formulas of physics laws change upon change of scale but maintain their mathematical form, thus exhibiting form invariance. As a result, using consistent units is essential in physics and leads to powerful dimensional estimates of the order of magnitude of physical quantities based on a simple dimensional analysis. The underlined scale is closely related to the presence of a material content, which reflects the energy scale involved.

Without matter, it is difficult to define a scale. Therefore, an empty universe would be expected to be scale invariant. This is confirmed by the scale invariance of Maxwell's equations in a vacuum, which are the equations that govern the dynamics of the electromagnetic fields. The field equations of general relativity are also scale invariant for empty space with zero cosmological constants. However, it is still an open question how much matter is needed to break scale invariance. This question is particularly relevant to cosmology and the evolution of the universe. Evidently, even a tiny amount of matter drastically reduces the effects of scale invariance; however, the effects only fully disappear for Ω_m equal and above 1 (see Section 3.1). Thus, for Ω_m between, 0.01 and 0.50, there are possibly some effects.

In this respect, key aspects or observations that distinguish SIV from the standard cosmological model based on the usual cosmological tests are the relations m-M vs. z, but the differences are very small, and there is no hope to solve the question rapidly. For low Ω_m, the values are a bit larger and could allow some differentiation. Redshift drifts (see Section 3.2) are likely the most powerful tests, but we have to wait for a decade or two. For now, the main effects concern the growth of density fluctuations (see Section 3.6), the rotation curves of galaxies, and the velocities in galaxy clusters.

1.2. Einstein General Relativity and Weyl Integrable Geometry

Einstein's general theory of relativity (EGR) is built upon the idea that a torsion-free covariant connection is both metric-compatible and maintains the length of vectors along geodesics. This theory has been extensively tested and validated across various scales, from local Earth-based laboratories to the vast expanse of the cosmos. Its validity has been confirmed at the solar system level through light-bending effects, at galactic scales through the observation of gravitational waves, and even beyond our own galaxy. EGR serves as the cornerstone of modern cosmology and astrophysics. However, at galactic and cosmic scales, peculiar and unexplained phenomena have emerged. These phenomena are often attributed to the presence of unknown matter particles or fields that remain undetected in our laboratories, hence the enigmatic terms "dark matter" and "dark energy".

Since no new particles or fields have been detected in Earth labs for more than twenty years, it is reasonable to revisit some old ideas that have been proposed as modifications of Einstein's general relativity. In 1918, Weyl proposed an extension by adding local gauge (scale) invariance [11]. Other approaches were more radical, such as Kaluza–Klein unification theory, which adds extra dimensions. The return to the usual 4D spacetime could be done using projective relativity theory via Jordan conformal equivalence, but with at least one additional scalar field. Such theories are also known as Jordan–Brans–Dicke (JBD) scalar-tensor gravitation theories [12–14]. In general, there is a body of research on "tensor-scalar theories" with local conformal invariance, i.e., Jackiw and Pi [15], pointing out that there is "No New Physics in Conformal Scalar-Metric Theory" by Tsamis and Woodard [16]. There is no contradiction of the SIV theory with these results, since there is no specific scalar field within the SIV beyond the conformal transformation factor λ. In most JBD theories, there is a major drawback: a varying Newton constant G. Some theories go even further to consider spatially varying G gravity [17]. No such variations have been observed yet, so we prefer to view Newton's gravitational constant G as constant despite some current experimental issues [18].

The discussion above raises the intriguing possibility that the enigmatic "dark" phenomena could be artifacts of a non-zero change in the length of vectors along geodesics. While this change is typically negligible and close to zero, $(\delta \| \overrightarrow{v} \| \approx 0)$, it could accumulate over vast cosmic distances, leading to the illusion of dark matter and/or dark energy. As a further generalization of Einstein's general relativity (EGR) paradigm, Weyl proposed an extension that incorporates local gauge (scale) invariance, a desirable property [11]. This extension allows for the possibility of length changes during parallel transport. However, initial concerns arose regarding the path-dependent nature of such a model, potentially contradicting observations. To address this objection, Weyl integrable geometry (WIG) was introduced [19,20], where the conservation of vector lengths is restricted to closed paths. $(\oint \delta \| \overrightarrow{v} \| = 0)$.

This concept paves the way for scale-invariant cosmology, as envisioned by Dirac and Canuto in their respective works, Dirac [19], Canuto et al. [20]. This formulation effectively resolves Einstein's objection to Weyl's original idea. Moreover, since our observations of the distant universe are limited to the waves that reach us, the condition for Weyl integrable geometry essentially implies that the information we receive through different paths constructively interferes, producing a coherent picture of the source.

The construction of a Weyl integrable geometry (WIG) involves applying a conformal transformation to the metric field $(g_{\mu\nu} \to \lambda^2 g_{\mu\nu})$ and examining its implications for various observational phenomena. As we will explore in the following discussion, the requirement for a homogeneous and isotropic space restricts the field λ to be solely dependent on cosmic time, independent of spatial coordinates. In such models there is additional acceleration in the equations of motion directly proportional to the particle's velocity.

Such behavior is somewhat similar to that of Jordan–Brans–Dicke's scalar-tensor gravitation, but the conformal factor λ does not appear to be a typical scalar field as in the Jordan–Brans–Dicke theory [12,13]. Furthermore, the Scale-Invariant Vacuum Vacuum (SIV)

concept provides a way to determine the specific functional form of $\lambda(t)$ as it applies to FLRW cosmology and its WIG extension.

The functional form of λ leads to a specific functional form for the rate of change of its logarithm $\kappa = -d(\ln \lambda)/dt$, which controls the strength of an additional SIV acceleration κv in the SIV-modified equations of motion. It is important to note that the additional acceleration in the equations of motion, which is proportional to the velocity of a particle, can also be justified by requiring reparametrization symmetry. Reparametrization invariance is often overlooked as being part of the general covariance that guarantees that physics is independent of the observer's coordinate system. However, reparametrization symmetry is much more than that; it is about the physics being independent of the choice of parametrization of a process under study. Not implementing reparametrization invariance in a model could lead to un-proper time parametrization. *The proper time parametrization of a process is the time, up to a constant scale factor, measured by a standard clock in the rest/co-moving inertial frame for the process. Any other time parametrization will be considered un-proper time parametrization since it is arbitrary. In this respect, the coordinate time of any arbitrary coordinate system will provide an example of un-proper time parametrization for the process when described in that coordinate frame.* Note, that we use the word "un-proper" instead of "improper" since what is improper usually depends on the social context and may have more than one occasions when something improper and wrong is actually proper and ok in many other contexts. In this respect un-proper is usually not the proper time parametrization in general but it is not actually wrong since reparametrization invariance allows one to use any reasonable parametrization choices. Such un-proper time parametrization seems to induce "fictitious forces" in the equations of motion, similar to the forces derived in the weak-field SIV regime [10]. This is a puzzling observation that may help us better understand nature, given its relation to some of the key properties of physical systems [21].

In short, the Scale-Invariant Vacuum (SIV) paradigm is an extension of the standard Einstein general relativity (EGR) theory, by the inclusion of an additional symmetry, on the basis of Weyl's integrable geometry (WIG). The SIV paradigm introduces a scale-invariant length scale, which is determined by the functional form of the vacuum energy density. This scale-invariance leads to a modified form of the equations of motion and an additional acceleration term, which can also be justified by reparametrization symmetry. This additional acceleration term is proportional to the velocity of a particle and can explain phenomena such as dark matter and dark energy. Overall, the SIV paradigm offers a new perspective on the fundamental principles of gravity and cosmology.

2. Mathematical Framework

The framework for the Scale-Invariant Vacuum paradigm is based on the Weyl integrable geometry and Dirac co-calculus as mathematical tools for the description of nature [11,19]. For a more modern treatment of the scale-invariant gravity idea, see [22], which is based on Cartan's formalism and along the more traditional scalar field approach, which, due to its abstractness, seems to have stayed disconnected from observational tests, apart from a few papers on the model parameters for conformal cosmology [23,24] where dark matter and energy seem to be replaced by the concept of rigid matter, which is still observationally questionable as its dark counterparts. Other unreasonable ideas are related to tired light or varying speed of light considerations [25,26], which seem to be relevant to the general Weyl mathematically framework, but do not account for the current view for defining the International System of Units [27]. Here, our approach is more traditional, physically motivated and with as little general abstraction as possible. For more mathematical details, we refer the reader to the companion paper on the "Action Principle for Scale Invariance and Applications (Part I)" [9].

The key distinctions between the mathematical framework and conceptual foundations between the EGR and WIG are the use of Weyl integrable geometry and Dirac co-calculus in the Scale-Invariant Vacuum paradigm, whereas the traditional approach relies on Einstein's general relativity. Additionally, the concept of reparametrization invari-

ance is emphasized in the Scale-Invariant Vacuum paradigm, which is not as prominent in the traditional approach.

2.1. Weyl Integrable Geometry and Dirac Co-Calculus

The original Weyl geometry uses a metric tensor field $g_{\mu\nu}$, along with a "connexion" vector field κ_μ, and a scalar field λ. Here, we use the French spelling of the word connection to avoid misinterpretation and confusion with the usual meaning and use of a connection vector field. In Weyl integrable geometry, the "connexion" vector field κ_μ is not an independent field, but it is derivable from the scalar field λ.

$$\kappa_\mu = -\partial_\mu \ln(\lambda) \tag{1}$$

This form of the "connexion" vector field κ_μ guarantees its irrelevance, in the covariant derivatives, upon integration over closed paths. That is, $\oint \kappa_\mu dx^\mu = 0$. In other words, $\kappa_\mu dx^\mu$ represents a closed one-form; furthermore, it is an exact form, as (1) implies $\kappa_\mu dx^\mu = -d \ln \lambda$. Thus, the scalar function λ plays a key role in Weyl integrable geometry. Its physical meaning is related to the freedom of choice of a local scale gauge. Thus, λ relates to the changes in the equations of a physical system upon change in scale via local rescaling $l' \to \lambda(x)l$. Such a change could be induced via a local conformal transformation of the coordinates, in which case it is part of the general diffeomorphism symmetry, or it could be only a metric conformal transformation without any associated coordinate transformation.

2.1.1. Gauge Change and (Co-)Covariant Derivatives

The covariant derivatives utilize the rules of Dirac co-calculus [19] where tensors also have co-tensor powers based on the way they transform upon change of scale. For the metric tensor $g_{\mu\nu}$, this power is $\Pi(g_{\mu\nu}) = 2$. This follows from the way the length of a line segment ds is defined via the usual expression $ds^2 = g_{\mu\nu}dx^\mu dx^\nu$.

$$l' \to \lambda(x)l \Leftrightarrow ds' = \lambda ds \Rightarrow g'_{\mu\nu} = \lambda^2 g_{\mu\nu}.$$

Thus, $g^{\mu\nu}$ has co-tensor power of $\Pi(g^{\mu\nu}) = -2$ in order to make the Kronecker δ a scale-invariant object ($g_{\mu\nu}g^{\nu\rho} = \delta^\rho_\mu$). That is, a co-tensor is of power n when, upon local scale change, it satisfies

$$l' \to \lambda(x)l : \; Y'_{\mu\nu} \to \lambda^n Y_{\mu\nu} \tag{2}$$

2.1.2. Dirac Co-Calculus

In Dirac co-calculus, this results in the appearance of the "connexion" vector field κ_μ in the covariant derivatives of scalars, vectors, and tensors (see Table 1):

Table 1. Derivatives for co-tensors of power n.

Co-Tensor Type	Mathematical Expression
co-scalar	$S_{*\mu} = \partial_\mu S - n\kappa_\mu S,$
co-vector	$A_{\nu*\mu} = \partial_\mu A_\nu - {}^*\Gamma^\alpha_{\nu\mu} A_\alpha - n\kappa_\nu A_\mu,$
co-covector	$A^\nu_{*\mu} = \partial_\mu A^\nu + {}^*\Gamma^\nu_{\mu\alpha} A^\alpha - nk^\nu A_\mu.$

where the usual Christoffel symbol $\Gamma^\nu_{\mu\alpha}$ is replaced by

$${}^*\Gamma^\nu_{\mu\alpha} = \Gamma^\nu_{\mu\alpha} + g_{\mu\alpha}k^\nu - g^\nu_\mu \kappa_\alpha - g^\nu_\alpha \kappa_\mu. \tag{3}$$

The corresponding equation of the geodesics within the WIG was first introduced in 1973 by Dirac [19] and, in the weak-field limit, was re-derived in 1979 by Maeder and Bouvier [28] ($u^\mu = dx^\mu/ds$ is the four-velocity):

$$u^\mu_{*\nu} = 0 \Rightarrow \frac{du^\mu}{ds} + {}^*\Gamma^\mu_{\nu\rho} u^\nu u^\rho + \kappa_\nu u^\nu u^\mu = 0\,. \tag{4}$$

This geodesic equation has also been derived from reparametrization-invariant action in 1978 by Bouvier and Maeder [29]:

$$\delta\mathcal{A} = \int_{P_0}^{P_1} \delta(d\widetilde{s}) = \int \delta(\beta ds) = \int \delta\left(\beta \frac{ds}{d\tau}\right) d\tau = 0.$$

2.2. Consequences of Going beyond the EGR

Before we go into specific examples, such as FLRW cosmology and weak-field limit, there are some remarks to be made. By using (3) in (4), one can see that the usual EGR equations of motion receive extra terms proportional to the four-velocity and its normalization:

$$\frac{du^\mu}{ds} + \Gamma^\mu_{\nu\rho} u^\nu u^\rho = (\kappa \cdot u) u^\mu - (u \cdot u)\kappa^\mu \tag{5}$$

In the weak-field approximation within the SIV, one assumes an isotropic and homogeneous space for the explicit derivation of the new terms beyond the usual Newtonian Equations [29]. As seen from (5), the result is a velocity-dependent extra term $\kappa_0 \vec{v}$ with $\kappa_0 = -\dot{\lambda}/\lambda$, while the special components are set to zero ($\kappa_i = 0,\ i = 1,2,3$) due to the assumption of isotropic and homogeneous space. At this point, it is important to stress that the usual normalization for the four-velocity, $u \cdot u = \pm 1$ with sign related to the signature of the metric tensor $g_{\mu\nu}$, is a special choice of parametrization—the proper time parametrization τ. We denote a general parametrization in (5) with s, while τ is reserved for the proper time, and t is the coordinate-time parametrization.

A similar extra term ($\kappa_0 \vec{v}$) was recently obtained [10] as a consequence of reparametrization-invariant mathematical modeling but without the need for a weak-field approximation. That is, insisting on reparametrization symmetry for the equations of motion demands such term to be present in order to account for the change of parametrization within a chosen coordinate system. Within the proper time parametrization one usually has $\kappa_0 = 0$. However, if one assumes that the equations used for the process under study are parametrized via the proper time parametrization but rely on the observer coordinate time, without including the appropriate κ-term, then, one obtains incorrect modeling with un-proper time parametrization instead because coordinate time is often quite different from the proper time of a process. *Therefore, not accounting for reparametrization symmetry leads to missing terms in the mathematical formulas utilized in the modeling of a system.* The κ-term is required by reparametrization symmetry. When properly accounted for, it appears as a velocity-dependent fictitious acceleration [10]. The term $\kappa_0 \vec{v}$ is necessary to restore the broken symmetry, which is the reparametrization invariance of the process under consideration. To demonstrate this, we can apply an arbitrary time reparametrization $\lambda = dt/ds$. Then, the first term on the left-hand side of Equation (5) becomes

$$\lambda \frac{d}{dt}\left(\lambda \frac{d\vec{r}}{dt}\right) = \lambda^2 \frac{d^2\vec{r}}{dt^2} + \lambda\dot{\lambda}\frac{d\vec{r}}{dt}. \tag{6}$$

By moving the velocity-linear term to the right-hand side of (5), using $\kappa(t) = -\dot{\lambda}/\lambda$ after dividing by λ^2, we obtain a $\kappa_0\vec{v}$-like term on the right-hand side. If we perform this manipulation in the absence of the $\kappa_0\vec{v}$ term on the left-hand side of (5), the term is generated. If the $\tilde{\kappa}$ term is present in the equations, it is transformed into $\tilde{\kappa} \to \kappa + \tilde{\kappa}$.

Unlike in the SIV, where the time reparametrization $\lambda(t)$ is typically justified to be t_0/t, for reparametrization symmetry, the time dependence of $\lambda(t)$ can be arbitrary. As mentioned in [10], the additional term is not anticipated to appear when the time parametrization of the process coincides with the system's proper time. Consequently, a term of the form $\kappa\vec{v}$ can be interpreted as a crucial component for restoring reparametrization symmetry; while, when neglected, then it is an indicator of a broken reparametrization symmetry for the un-proper time parametrization of a process.

In the context of FLRW cosmology, under the assumption of homogeneity and isotropy of space, the proper time parametrization is given by $-c^2 d\tau^2 = -c^2 dt^2 + a(t)^2 d\Sigma^2$, where c is the speed of light (set to 1), Σ is a 3D space of uniform curvature, and $a(t)$ is the scale factor for the 3D space. Here, τ is the proper time of the cosmological evolution, while t is the coordinate time of an observer studying the cosmic evolution.

Upon transitioning to WIG, one introduces a multiplicative conformal factor $\lambda(x)$. In the case of $\lambda(t)$ (time dependence only), one can argue that this factor can be absorbed into $a(t)$ by redefining the coordinate time t via $d\tilde{t} = \lambda(t)dt$. However, this does not guarantee proper time parametrization in general. Therefore, it is likely that the FLRW cosmology equations with missing velocity-dependent terms will have un-proper time parametrization, unless one ensures that reparametrization symmetry is restored.

2.3. Scale-Invariant Cosmology

The scale-invariant cosmology equations, first introduced by Dirac in 1973 [19] and re-derived by Canuto in 1977 [20], are based on the corresponding expressions of the Ricci tensor and a relevant extension of the Einstein equations. We have recently revisited the topic to bring it into focus and aligned the SIV paradigm [9]. In what follows, we paint a broad-stroke picture of the equations and their consequences.

2.3.1. The Einstein Equation for Weyl's Geometry

Upon the metic conformal transformation $g'_{\mu\nu} = \lambda^2 g_{\mu\nu}$ from Weyl's framework to the EGR framework, where $g'_{\mu\nu}$ is the metric tensor in the EGR framework, a simple relation is induced between the Ricci tensor and scalar within Weyl's integrable geometry and the Einstein framework. In our convention, a prime ($\prime$) is used to denote EGR framework objects:

$$R_{\mu\nu} = R'_{\mu\nu} - \kappa_{\mu;\nu} - \kappa_{\nu;\mu} - 2\kappa_\mu\kappa_\nu + 2g_{\mu\nu}\kappa^\alpha\kappa_\alpha - g_{\mu\nu}\kappa^\alpha_{;\alpha}\,,$$
$$R = R' + 6\kappa^\alpha\kappa_\alpha - 6\kappa^\alpha_{;\alpha}\,.$$

By using these expressions, we can extent the standard EGR equation into

$$R_{\mu\nu} - \frac{1}{2}\,g_{\mu\nu}R = -8\pi G T_{\mu\nu} - \Lambda\, g_{\mu\nu}\,, \tag{7}$$

$$R'_{\mu\nu} - \frac{1}{2}\,g_{\mu\nu}R' - \kappa_{\mu;\nu} - \kappa_{\nu;\mu} - 2\kappa_\mu\kappa_\nu + 2g_{\mu\nu}\kappa^\alpha_{;\alpha} - g_{\mu\nu}\kappa^\alpha\kappa_\alpha = -8\pi G T_{\mu\nu} - \Lambda\, g_{\mu\nu}\,. \tag{8}$$

Here, Λ is in WIG and it is expected that $\Lambda = \lambda^2\Lambda_{\rm E}$, with $\Lambda_{\rm E}$ being the Einstein cosmological constant in EGR. This relationship guarantees the explicit scale invariance of the equations. This makes explicit the appearance of $\Lambda_{\rm E}$ as invariant scalar (in-scalar), since then, $\Lambda\, g_{\mu\nu} = \lambda^2\Lambda_{\rm E}\, g_{\mu\nu} = \Lambda_{\rm E}\, g'_{\mu\nu}$. That is, the co-scalar power of Λ in WIG is $\Pi(\Lambda) = -2$.

The equations above are a generalization of the original equations due to Einstein. As a result, there is a larger class of gauge symmetries, which must be fixed by an appropriate gauge choice in order to do practical studies. Dirac considered the large numbers hypothesis for their gauge choice [30]. Below, we consider a different gauge fixing.

The scale-invariant FLRW cosmology equations were first introduced in 1977 by Canuto et al. [20] in the following form:

$$\frac{8\,\pi G\varrho}{3} = \frac{k}{a^2} + \frac{\dot{a}^2}{a^2} + 2\,\frac{\dot{\lambda}\,\dot{a}}{\lambda\,a} + \frac{\dot{\lambda}^2}{\lambda^2} - \frac{\Lambda_{\rm E}\lambda^2}{3}\,, \tag{9}$$

$$-8\,\pi G p = \frac{k}{a^2} + 2\frac{\ddot{a}}{a} + 2\frac{\ddot{\lambda}}{\lambda} + \frac{\dot{a}^2}{a^2} + 4\frac{\dot{a}\,\dot{\lambda}}{a\,\lambda} - \frac{\dot{\lambda}^2}{\lambda^2} - \Lambda_{\rm E}\,\lambda^2\,. \tag{10}$$

The above equations reduce to the standard FLRW equations in the limit $\lambda = const = 1$. The scaling of Λ with λ has been utilized to revisit the cosmological constant problem within quantum cosmology [31]; this resulted in the conclusion that our universe is unusually

large, given that the mean size of all universes, where EGR holds, was calculated to be of the order of the Planck scale. In that study, $\lambda = const$ was a key assumption, as the various universes were expected to obey the EGR equations. The importance of going beyond $\lambda = const$ was already stressed in our previous review paper [1]: "what would be the expected mean size of a universe, if the condition $\lambda = const$ is relaxed, remains an open question for an ensemble of WIG-universes", and as such is still open.

2.3.2. The Scale-Invariant Vacuum Gauge at $T = 0$ and $R' = 0$

The idea of the Scale-Invariant Vacuum was first introduced in 2017 by Maeder [2]. For an empty universe model, the de Sitter metric is conformal to the Minkowski metric; thus, $R'_{\mu\nu}$ is a vanishing Maeder [2]. Therefore, for a conformally flat metric, that is, Ricci flat ($R'_{\mu\nu} = 0$) Einstein vacuum ($T_{\mu\nu} = 0$), the following vacuum equation can be obtained using (8):

$$\kappa_{\mu;\nu} + \kappa_{\nu;\mu} + 2\kappa_\mu\kappa_\nu - 2g_{\mu\nu}\kappa^\alpha_{;\alpha} + g_{\mu\nu}\kappa^\alpha\kappa_\alpha = \Lambda\, g_{\mu\nu} \tag{11}$$

For homogeneous and isotropic space ($\partial_i\lambda = 0$), only $\kappa_0 = -\dot{\lambda}/\lambda$ and its time derivative $\dot{\kappa}_0 = -\kappa_0^2$ can be non-zero. As a corollary of (11), one can derive the following set of Equations [2]:

$$3\,\frac{\dot{\lambda}^2}{\lambda^2} = \Lambda\,, \quad \text{and} \quad 2\frac{\ddot{\lambda}}{\lambda} - \frac{\dot{\lambda}^2}{\lambda^2} = \Lambda\,, \tag{12}$$

$$\text{or} \quad \frac{\ddot{\lambda}}{\lambda} = 2\,\frac{\dot{\lambda}^2}{\lambda^2}\,, \quad \text{and} \quad \frac{\ddot{\lambda}}{\lambda} - \frac{\dot{\lambda}^2}{\lambda^2} = \frac{\Lambda}{3}\,. \tag{13}$$

These equations can be derived by using the time and space components of the equations, or by looking at the relevant trace invariant along with the relationship $\dot{\kappa}_0 = -\kappa_0^2$. Any one pair among these equations is sufficient to prove the validity of the other pair of equations.

Theorem 1. *Using the SIV Equations* (12) *or* (13) *with* $\Lambda = \lambda^2\Lambda_E$*, one obtains*

$$\Lambda_E = 3\frac{\dot{\lambda}^2}{\lambda^4}, \quad \text{with} \quad \frac{d\Lambda_E}{dt} = 0. \tag{14}$$

Corollary 1. *The solution of the SIV gauge equations is then*

$$\lambda = t_0/t, \tag{15}$$

with $t_0 = \sqrt{3/(c^2\Lambda_E)}$ *where c is the speed of light, usually set to 1.*

The choice of such a gauge for λ can be used to replace the Dirac's large numbers hypothesis invoked by Canuto et al. [20]. This is what we refer to as a Scale-Invariant Vacuum (SIV) gauge for λ.

Even more, now, we can have an alternative viewpoint on (8) and (11). Since (8) is scale invariant, then one does not have to consider the zero case for $T_{\mu\nu}$ and $R_{\mu\nu}$ in general, but if the scale factor λ satisfies (11), then all the κ terms and the Λ term in (8) will cancel out, leaving us with the standard EGR equation with zero cosmological constants. *Thus, a proper choice of* λ *gauge satisfying* (11) *results in the standard Einstein equation with no cosmological constant!* This is easily seen in the case of a homogeneous and isotropic universe or when requiring only reparametrization invariance, then both cases result in (12) and (13) along with (14). *If one takes the reparametrization symmetry viewpoint, then the presence of a non-zero cosmological constant is an indication of un-proper time parametrization that can be cured upon a suitable new time gauge deduced by the appropriate choice of* λ.

Upon the use of the SIV gauge, first in 2017 by Maeder [2], one observes that *the cosmological constant disappears* from Equations (9) and (10):

$$\frac{8\,\pi G\varrho}{3} = \frac{k}{a^2} + \frac{\dot{a}^2}{a^2} + 2\,\frac{\dot{a}\dot{\lambda}}{a\lambda}\,, \tag{16}$$

$$-8\,\pi G p = \frac{k}{a^2} + 2\frac{\ddot{a}}{a} + \frac{\dot{a}^2}{a^2} + 4\frac{\dot{a}\dot{\lambda}}{a\lambda}\,. \tag{17}$$

Maeder [2] provides a detailed analysis of the solutions to these equations, along with various cosmological properties related to Hubble—Lemaître and deceleration parameters, cosmological distances, and different cosmological tests. Redshift drifts have emerged as one of the most promising cosmological tests [6]. In this paper, we focus on aspects specific to the topic at hand. Analytical solutions have been obtained for flat SIV models with $k = 0$, both for matter-dominated [32] and radiation-dominated [33] scenarios. The matter-dominated case yields a straightforward expression:

$$a(t) \;=\; \left[\frac{t^3 - \Omega_\mathrm{m}}{1 - \Omega_\mathrm{m}}\right]^{2/3}\,. \tag{18}$$

The usual SIV timescale t is used above, with the present time defined as $t_0 = 1$ and the scale factor at present as $a(t_0) = 1$. These solutions are discussed in Section 3.1. They closely resemble the ΛCDM solutions, with the discrepancies increasing for lower Ω_m values. There is a general observation: *"the effects of scale invariance become more pronounced at lower matter densities, reaching their maximum in the case of empty space"*, as emphasized in Maeder [34]. As usual, here, $\Omega_\mathrm{m} = \varrho/\varrho_\mathrm{c}$ with $\varrho_\mathrm{c} = 3H_0^2/(8\pi G)$. Remarkably, Equations (16) and (17) allow flatness for different values of Ω_m. It follows from (18) that the initial time at $a(t_\mathrm{in}) = 0$ is related to the value of Ω_m:

$$t_\mathrm{in} \;=\; \Omega_\mathrm{m}^{1/3}\,. \tag{19}$$

The Hubble parameter and $\kappa_0(t) = -\dot{\lambda}/\lambda$ are then, in the timescale t (which goes from t_in for the Big Bang to $t_0 = 1$ for the present),

$$H(t) = \frac{\dot{a}}{a} = \frac{2\,t^2}{t^3 - \Omega_\mathrm{m}}\,,\ \text{and}\ \kappa_0(t) = -\frac{\dot{\lambda}}{\lambda} = \frac{1}{t}. \tag{20}$$

From Equations (18) and (20), we see that there is no meaningful scale-invariant solution for an expanding universe ($H > 0$) with Ω_m equal or larger than 1. Thus, the model solutions are quite consistent with the causality relations discussed by Maeder and Gueorguiev [5].

The usual timescale τ in years or seconds is $\tau_0 = 13.8$ Gyr at present [35] and $\tau_\mathrm{in} = 0$ at the Big Bang. One can change from the SIV-time t to the usual timescale τ by using the relationship ansatz [7]

$$\frac{\tau - \tau_\mathrm{in}}{\tau_0 - \tau_\mathrm{in}} = \frac{t - t_\mathrm{in}}{t_0 - t_\mathrm{in}}\,, \tag{21}$$

which expresses that the age fraction with respect to the present age is the same in both timescales. This ansatz gives

$$\tau \;=\; \tau_0\,\frac{t - \Omega_\mathrm{m}^{1/3}}{1 - \Omega_\mathrm{m}^{1/3}} \quad \text{and} \quad t \;=\; \Omega_\mathrm{m}^{1/3} + \frac{\tau}{\tau_0}(1 - \Omega_\mathrm{m}^{1/3})\,, \tag{22}$$

The relevant derivatives are constants depending on $t_\mathrm{in} = \Omega_\mathrm{m}^{1/3}$ and τ_0 only:

$$\frac{d\tau}{dt} \;=\; \frac{\tau_0}{1 - \Omega_\mathrm{m}^{1/3}}\,, \quad \text{and} \quad \frac{dt}{d\tau} \;=\; \frac{1 - \Omega_\mathrm{m}^{1/3}}{\tau_0}\,. \tag{23}$$

For larger Ω_m, the timescale t is squeezed over a smaller fraction of the interval from 0 to 1 (which reduces the range of λ over the ages). Using the above expressions, one can write the Hubble parameter in the usual timescale τ via its expression in the t-scale:

$$H(\tau) = \frac{\dot{a}}{a} = H(t)\frac{dt}{d\tau} = H(t)\frac{1-\Omega_m^{1/3}}{\tau_0}. \tag{24}$$

This finally gives, for the Hubble constant,

$$H_0 = \frac{2}{1-\Omega_m}\frac{1-\Omega_m^{1/3}}{\tau_0}. \tag{25}$$

The last factor could be recognized as $\kappa_0(\tau_0)$. To see this, one can utilize Equations (22) and (23) to switch from the SIV-time t to the conventional time τ scale [7], in order to obtain

$$\kappa_0(\tau) = -\frac{\dot{\lambda}}{\lambda} = \kappa_0(t)\frac{dt}{d\tau} = \frac{1-t_{in}}{t\,\tau_0} = \frac{1-t_{in}}{\tau_0}\frac{1}{t_{in}+(1-t_{in})(\tau/\tau_0)} = \frac{\psi(\tau)}{\tau_0}, \tag{26}$$

$$\Rightarrow \kappa_0(\tau_0) = \frac{1-\Omega_m^{1/3}}{\tau_0} \text{ and } \psi(\tau) = \frac{1-t_{in}}{t_{in}+(1-t_{in})(\tau/\tau_0)}. \tag{27}$$

3. Comparisons and Applications

Over the past few years, the authors have published a series of papers that compare the predictions and outcomes of the SIV paradigm to observations. The main results and outcomes are discussed in this section.

3.1. Comparing the Scale Factor $a(t)$ within ΛCDM and the SIV [2]

The implications of the Scale-Invariant Vacuum Paradigm for cosmology were first discussed by Maeder [2] and later reviewed by Maeder and Gueorguiev [6]. In this paper, we use the SIV Equations (16) and (17), along with the gauge fixing (14), which implies (15), that is, $\lambda = t_0/t$ with t_0 indicating the current age of the universe since the Big Bang, defined as $a(t_{in}) = 0$ at some past moment t_{in}.

The most important point in comparing ΛCDM and SIV cosmology models is the existence of SIV cosmology with slightly different parameters but almost the same curve for the standard scale parameter $a(t)$ when the timescale is set, so that $t_0 = 1$ at the present epoch [2,6].

As seen in Figure 1, the differences between the ΛCDM and SIV models decline for increasing matter densities [2]. Furthermore, the SIV solutions lie relatively close to the ΛCDM ones, the differences being larger for lower Ω_m. This is a general property: *the effects of scale invariance are always larger for the lower matter densities, being the largest when approaching the empty space.*

Furthermore, from these results, one can expect that a SIV model that is to match the $a(t)$ for ΛCDM would require a slightly higher Ω_m value given the same time coordinate for both models. This means that, for observationally deduced expansion curves, higher values of Ω_m will be expected to be assigned by the SIV models than by the ΛCDM models. However, the time coordinates are not the same in these two theories. As usual, let us use primes to indicate EGR and non-primes for WIG quantities, then, if one is to consider $t' = \tau/\tau_0$ as ΛCDM model time and t as a SIV, then one should have $a' = \lambda\, a$ with λ related to the transition between the two time functions. This means that the SIV curve $\lambda\, a(t)$ will be further above the ΛCDM curve; however, the time t should be pushed to the right of t' due to the relation (22) and effectively bringing the $a - t$ curves of these two theories closer.

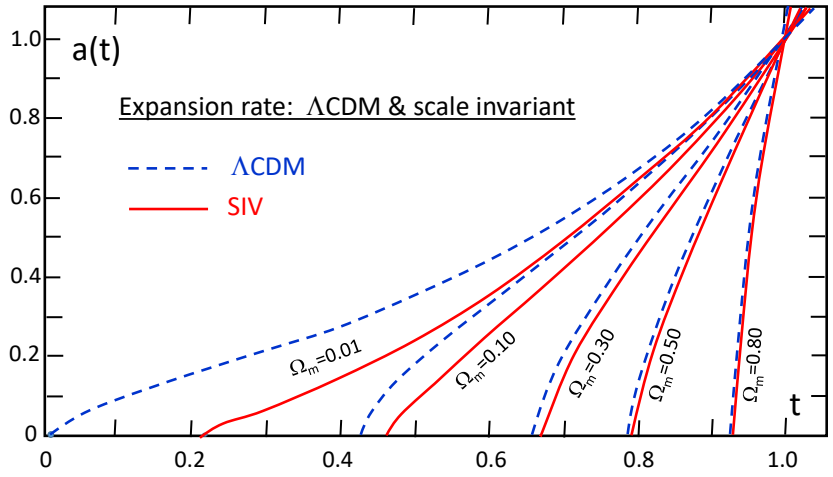


Figure 1. Expansion rates $a(t)$ as a function of time t in the flat ($k = 0$) ΛCDM and SIV models in the matter-dominated era. The curves are labeled by the values of $\Omega_{\rm m}$; here, $\Omega_{\rm m} = \varrho/\varrho_{\rm c}$ with $\varrho_{\rm c} = 3H_0^2/(8\pi G)$. Drawing originally published in [2]. The time parameter t is the dimensionless time chosen so that the current epoch is at $t_0 = 1$.

The above argument shows that what one may perceive as simple comparison between ΛCDM and the SIV is not actually that simple. It is more appropriate to compare the models to observations and to deduce the relevant parameters that provide agreement with the observations. In this respect, when comparing the age of the universe of 13.8 ± 0.7 Gyr and possible values of the Hubble constant in the range $65 \leq H_0 \leq 76$, one obtains $0.18 \leq \Omega_{\rm m} \leq 0.33$. For further studies and better understanding of the topic, we suggest the relevant discussion in Maeder [2] and, more specifically, a closer look at Figure 8 in [2].

3.2. Possible Differentiators of the SIV from ΛCDM [6]

The major property of SIV cosmology is that it naturally predicts an acceleration of the expansion. This is the consequence of the additional term in Equations (16) and (17), which predicts an acceleration of the motion in the direction of the velocity. If the universe were to contract, it would also receive an additional acceleration favoring a contraction.

Several observational tests of the SIV cosmology were performed and discussed in detail in [6]. For example, based on Figure 3 in [6], one can see that the relation between the Hubble constant H_0 and the age of the universe in SIV cosmology suggests a range of values for Ω_m between 0.15 and 0.25, depending on the choice for H_0 using either the distance ladder or Planck collaboration measurements.

Most cosmological tests, such as the magnitude–redshift, the angular diameter vs. redshift, the number count vs. redshifts, etc., depend on the expressions of the distances based on the angular diameters $d_{\rm A}$. The plot of $d_{\rm A}$ vs. z in Figure 2 shows that the different curves are not well separated at a lower z. At $z = 1$, for $\Omega_{\rm m} = 0, 0.1, 0.3, 0.99$, one, respectively, has $\log d_{\rm A} = -0.383, -0.367, -0.349, -0.342$. Up to a redshift $z = 2$, the relations between $d_{\rm A}$ and z for scale-invariant models are very close to each other, for any $\Omega_{\rm m}$, with a deviation from the mean smaller than ± 0.05 dex. For ΛCDM models, higher density models always have lower $d_{\rm A}$ with an increasing separation between the curves with an increasing z. For the SIV models, this is the same, however with a very small differentiation, up to only $z \approx 2$. Above 2, the SIV models behave differently: higher density models have larger $d_{\rm A}$ values. The above properties are evidently also shared by the magnitude–redshift, the angular diameter vs. redshift, as well as by number count plots. A clear discrimination between the SIV and ΛCDM models with an access to $\Omega_{\rm m}$ requires high-precision measurements at redshifts higher than 2.

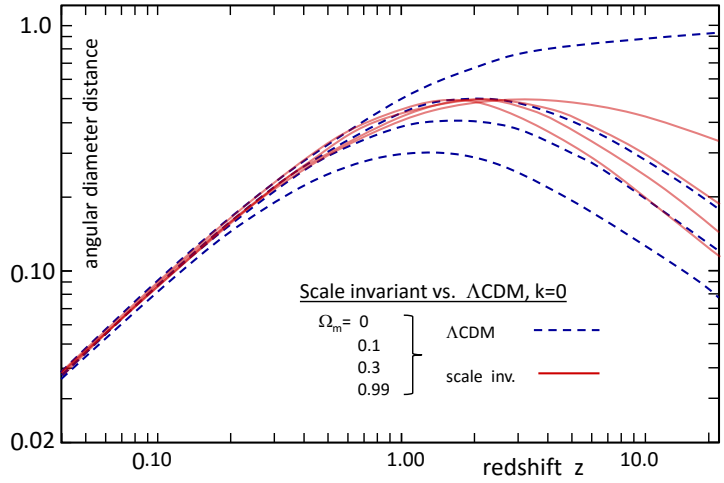


Figure 2. Angular diameter distance d_A vs. redshift z for flat scale-invariant models (continuous red lines) compared to flat ΛCDM models (broken blue lines). The curves are given for $\Omega_m = 0, 0.1, 0.3, 0.99$, from the upper to the lower curve in both cases (at $z > 3$). Original figure from Maeder [2].

Figure 3 shows the (m-M) vs. z plot based on SNIa, quasar, and GRB data by Lusso et al. [36] compared to different theoretical curves. The two red lines show the SIV models for $\Omega_m = 0.10$ and 0.30. This last model lies very close to the ΛCDM model with $\Omega_m = 0.30$, illustrating the above-mentioned difficulty to discriminate between the ΛCDM and SIV models. We note that the SIV models with $\Omega_m = 0.10$ better fits the high z points, which could perhaps support a lower value. However, internal effects in the evolution galaxies may also intervene in the comparison of distant and local galaxies, in addition to the cosmological effects and this imposes great care in the conclusions. Since the SIV Ω_m parameter is not yet well constrained, it seems adequate to anticipate that the final SIV curve would be somewhere between the two red curves shown in Figure 3.

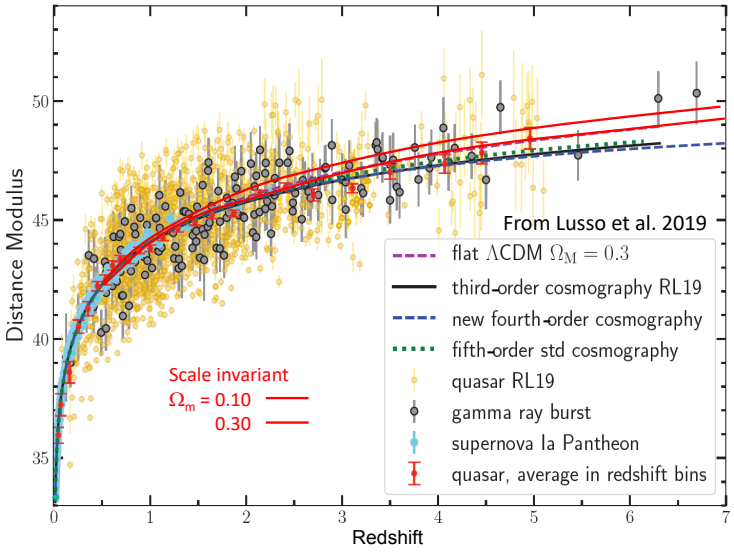


Figure 3. The Hubble diagram for SNIa, quasars (binned), and GRBs from the samples collected by Lusso et al. [36]. The various models considered by Lusso et al. are indicated. The two red lines show the flat scale-invariant models with $k = 0$ and $\Omega_m = 0.10$ and 0.30. Note that the ΛCDM and SIV models with $\Omega_m = 0.30$ are easily confused. The other lower curves are attempts of adjustments by series developments. Drawing originally published in [6].

Figure 4, below, shows the curves of the redshift drifts as a function of z predicted in the SIV cosmology for different values of Ω_m. (A z-drift is the change z for a given galaxy over time, a time interval longer than 20 yr appears necessary.) The SIV-drifts are compared to a few standard models of different Ω_Λ values by Liske et al. [37]. We notice the relative proximity of the standard and scale-invariant curves in the case of $\Omega_m = 0.30$, which could make the separation of models difficult for such a density parameter. However, the expected value of Ω_m in the SIV cosmology is likely significantly smaller than in the ΛCDM models; this makes the differences of the z-drifts between the two kinds of cosmological models possibly observable by very accurate observations in the future. The physical reason of these differences between the two models at a high z is due to the flatter initial expansion curve in the SIV models. In this respect, we recall that the empty SIV model expands with t^2, while the empty ΛCDM model is in fact a de Sitter model, which expands exponentially.

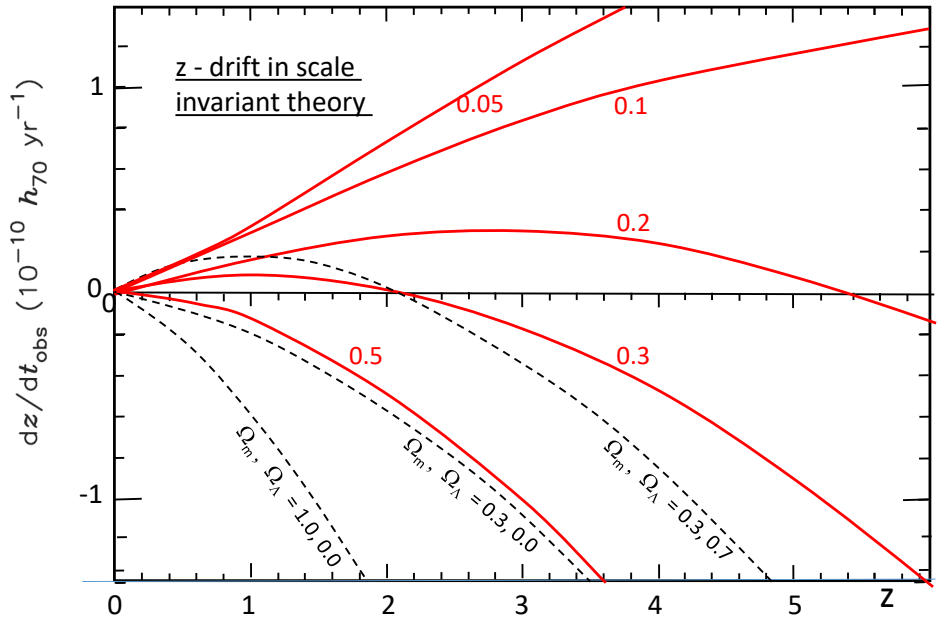


Figure 4. The drifts of redshifts dz/dt as a function of redshift in the scale-invariant theory (red curves). The values of Ω_m (usual definition) are indicated. The black broken lines give the results for some standard models of different couples $(\Omega_\Lambda, \Omega_m)$ by Liske et al. [37]. Drawing originally published in [6].

The above comparisons, see also [6], show a general agreement between SIV predictions and observations, just as for the ΛCDM models. The redshift drifts appear to have a particularly great differentiation power between the SIV and ΛCDM models.

3.3. Application to Scale-Invariant Dynamics of Galaxies [4]

The application of the SIV paradigm to scale-invariant dynamics of galaxies addresses the behavior of the velocity as a function of radius, i.e., the problem of the flat rotation curves, which was a major point leading to the concept of dark matter. It also addresses the problem of the too-high mean velocity in clusters of galaxies, which, in standard theory leads to too-high masses and dark matter as well. Here, however, we will focus on the Radial Acceleration Relation (RAR) within the SIV and its consequences for dwarf spheroidals.

A significant consequence of scale invariance at cosmic scales is the derivation of a universal formula for the Radial Acceleration Relation (RAR) between g_{obs} and g_{bar} [4]. This relation describes the connection between the observed gravitational acceleration, $g_{obs} = v^2/r$, and the acceleration attributed to baryonic matter through standard Newtonian gravity, g_N ($g = g_{obs}$, $g_N = g_{bar}$):

$$g = g_N + \frac{k^2}{2} + \frac{1}{2}\sqrt{4g_N k^2 + k^4}, \tag{28}$$

for $g_N \gg k^2 : g \to g_N$, but for $g_N \to 0 \Rightarrow g \to k^2$ is a constant.

As shown in Figure 5, MOND significantly deviates from the trend seen in dwarf spheroidals. This is a problem within MOND due to the different interpolating functions needed by MOND—one for galaxies and one for cosmic scales. The SIV expression (28) naturally resolves this issue by using only one universal parameter related to gravity at large distances [4].

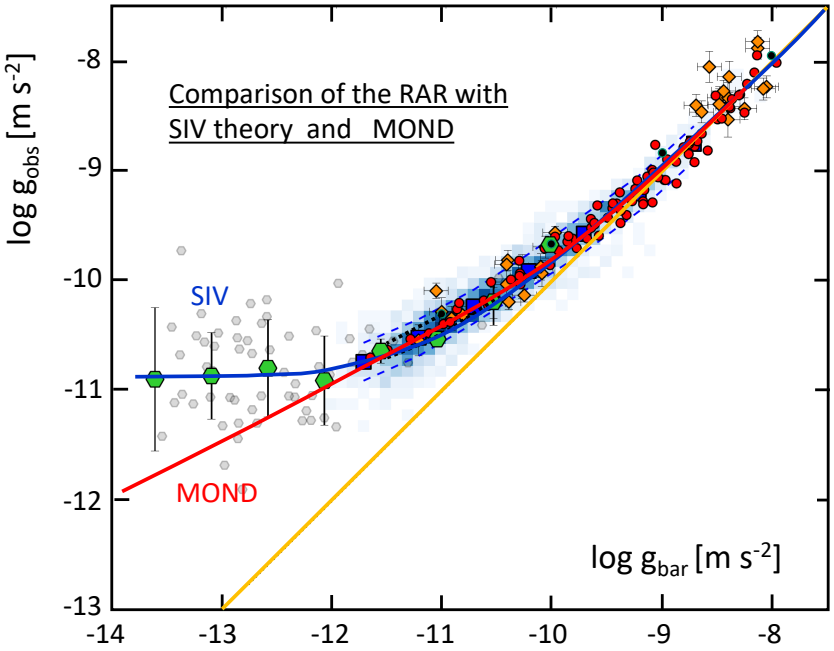


Figure 5. Radial Acceleration Relation (RAR) for the galaxies studied by Lelli et al. (2017). Dwarf spheroidals represented as binned data (big green hexagons), along with MOND (red curve), and SIV (blue curve) model predictions. The orange curve shows the 1:1 line for g_{obs} and g_{bar}. Due to the smallness of g_{obs} and g_{bar}, the application of the log function results in negative numbers; thus, the corresponding axes' values are all negative. Drawing originally published in [4].

The above Equation (28) is derived from the weak-field approximation of the SIV by using Dirac co-calculus in the derivation of the geodesic equation within the relevant WIG (4). For more details, see Maeder and Gueorguiev [4] and the original derivation in Maeder and Bouvier [28]:

$$\begin{aligned} g_{ii} = -1,\ g_{00} &= 1 + 2\Phi/c^2 \Rightarrow \Gamma^i_{00} = \frac{1}{2}\frac{\partial g_{00}}{\partial x^i} = \frac{1}{c^2}\frac{\partial \Phi}{\partial x^i}, \\ \frac{d^2\overrightarrow{r}}{dt^2} &= -\frac{G_t M}{r^2}\frac{\overrightarrow{r}}{r} + \kappa_0(t)\frac{d\overrightarrow{r}}{dt}. \end{aligned} \tag{29}$$

where $i \in \{1,2,3\}$, while the potential $\Phi = G_t M/r$ is scale invariant and G_t is Newton's constant of gravity in the SIV's time units system ($t_0 = 1$). When written in the usual units with present time τ_0, based on (27), the modified Newton's Equation (29) is then [7,34]

$$\frac{d^2\overrightarrow{r}}{d\tau^2} = -\frac{G\,M(\tau_0)}{r^2}\frac{\overrightarrow{r}}{r} + \frac{\psi_0}{\tau_0}\frac{d\overrightarrow{r}}{d\tau}\,. \tag{30}$$

By considering the scale-invariant ratio of the correction term $\kappa_0\, v$ to the usual Newtonian term in (29), one obtains

$$x = \frac{\kappa_0 v r^2}{GM} = \frac{H_0}{\xi}\frac{v\, r^2}{GM} = \frac{H_0}{\xi}\frac{(r\, g_{\rm obs})^{1/2}}{g_{\rm bar}} \sim \frac{g_{\rm obs} - g_{\rm bar}}{g_{\rm bar}}\,, \tag{31}$$

upon utilizing an explicit scale invariance, by considering ratios, to cancel the proportionality factor, we obtain

$$\left(\frac{g_{\rm obs} - g_{\rm bar}}{g_{\rm bar}}\right)_2 \div \left(\frac{g_{\rm obs} - g_{\rm bar}}{g_{\rm bar}}\right)_1 = \left(\frac{g_{\rm obs,2}}{g_{\rm obs,1}}\right)^{1/2}\left(\frac{g_{\rm bar,1}}{g_{\rm bar,2}}\right), \tag{32}$$

by setting $g = g_{\rm obs,2}$, $g_N = g_{\rm bar,2}$, and with $k = k_{(1)}$ containing all the system-1 terms, one finally obtains (28)

$$\frac{g}{g_{\rm N}} - 1 = k_{(1)}\frac{g^{1/2}}{g_{\rm N}} \Rightarrow g = g_{\rm N} + \frac{k^2}{2} \pm \frac{1}{2}\sqrt{4 g_{\rm N} k^2 + k^4}.$$

As it was noted already, $g_{\rm N} \gg k^2 : g \to g_{\rm N}$, but for $g_{\rm N} \to 0 \Rightarrow g \to k^2$ for the '+' branch, while the '−' branch gives $g \to 0$.

3.4. Mond as a Peculiar Case of the SIV Theory [34]

There are many developments of MOND into RMOND, QMOND, BIMOND, TRIMOND, as well as generalized Aether theories, TeVes, and other modified gravity and extended gravity theories, etc. [38–40], in an attempt to account for different properties and to generalize them. Here, however, the main point we wanted to emphasize is that the SIV, which rests on a unique and well-defined basis [9], gives an equation of motion (30) which, at gravities lower than a_0, provides results, for which MOND gives a valid approximation, however only over a limited range. However, the theory and the basic equations are different, despite their tangent behaviors over some domain of gravities.

The weak-field limit of the SIV tends to MOND when the scale factor is taken as constant, an approximation valid (< 1%) over the last 400 Myr. A better understanding of the MOND a_0-parameter in $g_{\rm obs} = \sqrt{a_0\, g_N}$ could be obtained within the SIV where it corresponds to the equilibrium point of the Newtonian and SIV dynamical acceleration [34]. The unique feature explained by the SIV theory is the relation known as the deep-MOND limit, where the resulting gravity is the square root of the product of the Newtonian gravity multiplied by a constant acceleration. This approximation is only valid at low gravities, when the additional "dynamic" acceleration becomes larger than Newtonian gravity. As such, the parameter a_0 is not a universal constant; it depends on the density and age of the universe. The first attempt at assessing possible z-dependence of a_0 was published recently [41].

In order to see the correspondence, one looks at $x\xi = H_0 \frac{v\, r^2}{GM}$ (31) in terms of densities: first, we consider the mass M as spherically distributed in a radius r with a mean density $\varrho = 3M/(4\pi r^3)$; then, we use $\varrho_{\rm c} = \frac{3H_0^2}{8\pi G} \Rightarrow H_0 = \sqrt{8\pi G \rho_c/3}$, along with the instantaneous radial accelerator relation $\frac{v^2}{r} = \frac{GM}{r^2} \Rightarrow v = \sqrt{GM/r}$, to arrive at the expression $x\xi = \sqrt{2\rho_c/\rho}$. Since Newtonian gravity for a density ρ is $g_N = (4/3)\pi G\, \varrho\, r$, this translates into $x\xi = \sqrt{2g_c/g_N}$. Then, one can write (30) as

$$g = g_{\rm N} + x\, g_{\rm N} \to x\, g_{\rm N} = \frac{\sqrt{2}}{\xi}\left(\frac{g_{\rm c}}{g_{\rm N}}\right)^{1/2} g_{\rm N} = \frac{1}{\xi}\sqrt{2 g_{\rm c} g_{\rm N}}. \tag{33}$$

Therefore, one obtains the correspondence $a_0 \iff 2g_{\rm c}/\xi^2$, where $\xi = H_0/\kappa_0$. Thus, by using the SIV time t, where $\kappa_0(t) = 1/t$ due to (15), along with (20), one obtains $\xi = 2/(1 - \Omega_{\rm m})$, which, finally, gives

$$a_0 \iff \frac{(1-\Omega_m)^2}{2} g_c \,. \tag{34}$$

One may express the limiting value g_c in terms of the critical density over the radius r_{H_0} of the Hubble sphere. Thus, r_{H_0} is defined via $n\,c = r_{H_0} H_0$, where n depends on the cosmological model. For the EdS model, $n = 2$, while for the SIV or ΛCDM models with $\Omega_m = 0.2 - 0.3$, the initial braking and recent acceleration almost compensate each other, so that $n \simeq 1$. By using the expression for H_0 (25), one finally obtains

$$a_0 = \frac{(1-\Omega_m)^2}{2} \frac{4\pi}{3} G \varrho_c r_{H_0} = \frac{(1-\Omega_m)^2}{4} n\,c\,H_0 = \frac{n\,c\,(1-\Omega_m)(1-\Omega_m^{1/3})}{2\,\tau_0}. \tag{35}$$

Thus, the deep-MOND limit is found [34] to be an approximation of the SIV theory for low enough densities and for systems with timescales smaller than a few Myr, where λ can be viewed as if it is a constant.

The product $c\,H_0$ is equal to $6.80 \cdot 10^{-8}$ cm s^{-2}. For Ω_m = 0, 0.10, 0.20, 0.30, and 0.50, one obtains $a_0 \approx (1.70, 1.36, 1.09, 0.83, 0.43) \cdot 10^{-8}$ cm s^{-2}, respectively. These values obtained from the SIV theory are remarkably close to the value a_0 of about $1.2 \cdot 10^{-8}$ cm s^{-2} as derived from observations by Milgrom [42]. Thus, as emphasized in Maeder [34], we can conclude the following:

"... as it comes out for the more general SIV theory, there are several remarks to be made on the a_0-parameter and its meaning:

1. *The equation of the deep-MOND limit is reproduced by the SIV theory both analytically and numerically if λ and M can be considered as constant. This may apply to systems with a typical dynamical timescale up to a few hundred million years.*
2. *Parameter a_0 is not a universal constant. It depends on the Hubble–Lemaître H_0 parameter (or the age of the universe) and on Ω_m in the model universe, cf. Equation (35). The value of a_0 applies to the present epoch.*
3. *Parameter a_0 is defined by the condition that $x > 1$, i.e., when the dynamical gravity $\kappa_0 v = (\psi_0 v)/\tau_0$ in the equation of motion (30) becomes larger than the Newtonian gravity. This situation occurs in regions at the edge of gravitational systems".*

3.5. Local Dynamical Effects within the SIV: The Lunar Recession [7]

As previously mentioned, scale invariance is expected in cosmological models devoid of matter, while its presence tends to diminish this property. Indeed, scale invariance is unequivocally absent in cosmological models with densities equal to or exceeding the critical value $\varrho_c = 3H_0^2/(8\pi G)$ [5]. Evidently, the introduction of matter effectively nullifies scale invariance, as demonstrated in [43]. However, for models with densities below the critical value ϱ_c, the possibility of limited residual effects remains open. If scale invariance persists, it would manifest as a global cosmological property, with potential local observations. In the case of the Earth–Moon two-body system, the predicted additional lunar recession would increase by 0.92 cm/yr, accompanied by a slight enhancement in tidal interactions [7].

The Earth–Moon distance, meticulously measured since 1970 using the Lunar Laser Ranging (LLR) experiment, is the most precisely determined distance in the solar system. LLR measurements indicate a lunar recession of 3.83 (±0.009) cm/yr, corresponding to a tidal change in the length-of-day (LOD) of 2.395 ms/cy [44,45]. Remarkably, the observed lunar recession has remained consistent since its first determination over three decades ago [46], a testament to the high precision of LLR measurements. However, the observed change in LOD since Babylonian Antiquity is only 1.78 ms/cy [47], a result corroborated by paleontological data [48]. This discrepancy translates to a lunar recession of 2.85 cm/yr. Stephenson et al. [47] conducted the most extensive and rigorous studies on LOD changes, analyzing lunar and solar eclipses from 720 BC to 1600 AD. Their findings reveal an average LOD shift of 1.78 (±0.03) ms/cy. Stephenson et al. [49] further underscored the significance

of this discrepancy between the observed mean LOD (1.78 ms/cy) and the value predicted by tidal interactions (2.395 ms/cy).

The substantial difference of $(3.83 - 2.85)\,\mathrm{cm/yr} = 0.98\,\mathrm{cm/yr}$, consistently observed over the past two decades [50,51], aligns remarkably with the predictions of the scale-invariant theory, further supported by multiple astrophysical tests [7]. This discrepancy, bolsters the theory's validity and suggests a more accurate description compared to standard models. Further investigations could unlock deeper insights into the universe's fundamental laws, but one has to be careful to apply the correct SIV treatment otherwise one can make an error us done by Banik and Kroupa concerning the Lunar Motion within the SIV theory (see Appendix A for more details.)

By using the correct treatment of the Earth–Moon tidal interaction within the SIV theory, one derives an additional term in the equation describing the lunar recession in current time units [7]:

$$\frac{dR}{d\tau} = k_{\mathrm{E}} \frac{dT_{\mathrm{E}}}{d\tau} - k_{\mathrm{E}}\, \psi_0 \frac{T_{\mathrm{E}}}{\tau_0} + \psi_0 \frac{R}{\tau_0}. \tag{36}$$

In a cosmological model with $\Omega_{\mathrm{m}} = 0.30$, the ratio $\psi_0 = \frac{(t_0 - t_{\mathrm{in}})}{t_0} = 0.331$ (27). We use the following numerical values of the relevant astronomical quantities:

$$\begin{aligned} M_{\mathrm{E}} &= 5.973 \cdot 10^{27}\ \mathrm{g}, \qquad R_{\mathrm{E}} = 6.371 \cdot 10^{8}\ \mathrm{cm}, \\ M_{\mathrm{M}} &= 7.342 \cdot 10^{25}\ \mathrm{g}, \qquad R = 3.844 \cdot 10^{10}\ \mathrm{cm}, \\ I_{\mathrm{E}} &= 0.331 \cdot M_{\mathrm{E}} R_{\mathrm{E}}^2 = 8.0184 \cdot 10^{44}\ \mathrm{g \cdot cm^2}. \end{aligned} \tag{37}$$

The value 0.331 is obtained from precession data [52]. The coefficient k_{E} is estimated to be $1.60 \cdot 10^5\ \mathrm{cm \cdot s^{-1}}$ [7,53].

Let us numerically evaluate the various contributions. With the LOD of 1.78 ms/cy from the antique data by [47], the first term contributes to a lunar recession of 2.85 cm/yr. The second term in (36) gives, for the case of $\Omega_{\mathrm{m}} = 0.3$,

$$0.33 \cdot k_E \frac{T_{\mathrm{E}}}{\tau_0} = 0.33 \cdot 1.60 \cdot 10^5\ \mathrm{cm \cdot s^{-1}}\ \frac{86{,}400\ \mathrm{s}}{13.8 \cdot 10^9\ \mathrm{yr}} = 0.33 \left[\frac{\mathrm{cm}}{\mathrm{yr}}\right]. \tag{38}$$

The direct SIV expansion effect $\kappa_0 R = \psi_0 R/\tau_0$ is

$$0.33 \cdot \frac{R}{\tau_0} = 0.33 \cdot \frac{3.844 \cdot 10^{10}\,\mathrm{cm}}{13.8 \cdot 10^9\ \mathrm{yr}} = 0.92 \left[\frac{\mathrm{cm}}{\mathrm{yr}}\right]. \tag{39}$$

This term corresponds to a third of the general Hubble–Lemaître expansion. Summing the various contributions, we get the following historical data values [47]:

$$\begin{aligned} \text{for } \Omega_{\mathrm{m}} = 0.3, \text{ one obtains: } \tfrac{dR}{d\tau} &= (2.85 - 0.33 + 0.92)\,\mathrm{cm/yr} = 3.44\,\mathrm{cm/yr}, \\ \Omega_{\mathrm{m}} = 0.1, \text{ this is: } \tfrac{dR}{d\tau} &= (2.85 - 0.54 + 1.49)\,\mathrm{cm/yr} = 3.80\,\mathrm{cm/yr}, \\ \Omega_{\mathrm{m}} = 0.05, \text{ this is: } \tfrac{dR}{d\tau} &= (2.85 - 0.63 + 1.76)\,\mathrm{cm/yr} = 3.98\,\mathrm{cm/yr}. \end{aligned} \tag{40}$$

Thus, we see that the scale-invariant analysis gives a relatively good agreement with the lunar recession of 3.83 cm/yr obtained from LLR observations. The difference amounts to only 10% of the observed lunar recession for $\Omega_{\mathrm{m}} = 0.3$. Moreover, a low value of $\Omega_{\mathrm{m}} = 0.1$ is to better reconcile these values.

The difference in the lunar recession is well accounted for within the dynamics of the SIV theory (40). *At a minima,* the above results show that the problem of scale invariance is worthy of some attention within the solar system as well. Thus, what is accounted for by the SIV theory is the fact that, in the standard theory, the rate at which the Moon is receding is not consistent with the rate of the slowing down of the Earth since the time of the Babylonians. In the SIV, the two values are consistent.

3.6. Growth of the Density Fluctuations within the SIV [3]

The SIV paradigm suggests that the density fluctuations in the universe grow at a much faster rate compared to the Einstein–de Sitter model. This is due to the fact that the SIV theory incorporates scale invariance, which allows for a more rapid growth of these fluctuations due to the dynamical gravity term in the equations of motion (see Equation (29)). This is evident in the results shown in Figure 6, which depicts the growth of density fluctuations over time. The SIV theory also suggests that this growth is in a non-linear regime for redshifts above 2.5. The exact mechanisms or processes behind this rapid growth are still being studied, but it is believed that the equations of the scale invariance of the SIV theory allow for a more efficient transfer of energy and matter within the universe, leading to a faster growth of density fluctuations. That is, an essential effect in the fast growth of the density fluctuations is the fact that, in the SIV, the equation of motion contains an additional acceleration in the direction of motion. In the case of the contraction of a bulk of matter, this speeds up the corresponding collapse. Additionally, the SIV theory has been shown to be consistent with the observed data on highly redshifted galaxies, further supporting its explanation for the growth of density fluctuations in the early universe.

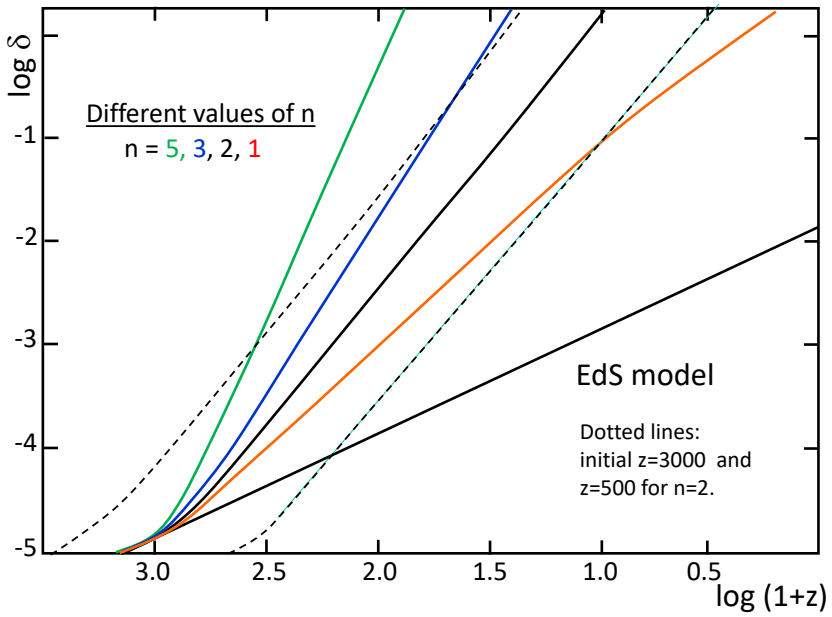


Figure 6. The growth of density fluctuations for different values of parameter n (the gradient of the density distribution in the nascent cluster) for an initial value $\delta = 10^{-5}$ at $z = 1376$ and $\Omega_{\rm m} = 0.10$. The initial slopes are those of the EdS models. The two light broken curves show models with an initial $(z + 1) = 3000$ and 500, with the same $\Omega_{\rm m} = 0.10$ and $n = 2$. These dashed lines are to be compared to the black continuous line of the $n = 2$ model. All three lines for $n = 2$ are very similar and nearly parallel. Due to to the smallness of δ, the application of the log function results in negative numbers; thus, the corresponding vertical axes values are all negative. Figure reprinted with permission from Maeder and Gueorguiev [3], Copyright 2019 Elsevier.

Another interesting finding was the potential for rapid growth of density fluctuations within the SIV [3]. Our study appropriately modified the following relevant equations: the continuity equation, Poisson equation, and Euler equation, within the SIV framework. Below are outlined the corresponding equations and the relevant results. Using the notation $\kappa = \kappa_0 = -\dot{\lambda}/\lambda = 1/t$, the corresponding continuity, Poisson, and Euler equations are

$$\frac{\partial \rho}{\partial t} + \vec{\nabla} \cdot (\rho \vec{v}) = \kappa \left[\rho + \vec{r} \cdot \vec{\nabla} \rho \right], \ \vec{\nabla}^2 \Phi = \triangle \Phi = 4\pi G \varrho,$$

$$\frac{d\vec{v}}{dt} = \frac{\partial \vec{v}}{\partial t} + \left(\vec{v} \cdot \vec{\nabla} \right) \vec{v} = -\vec{\nabla} \Phi - \frac{1}{\rho} \vec{\nabla} p + \kappa \vec{v}.$$

For a density perturbation $\varrho(\vec{x},t) = \varrho_b(t)(1+\delta(\vec{x},t))$, the above equations result in:

$$\dot{\delta} + \vec{\nabla}\cdot\dot{\vec{x}} = \kappa\vec{x}\cdot\vec{\nabla}\delta = n\kappa(t)\delta \quad , \quad \vec{\nabla}^2\Psi = 4\pi G a^2 \varrho_b \delta, \tag{41}$$

$$\ddot{\vec{x}} + 2H\dot{\vec{x}} + (\dot{\vec{x}}\cdot\vec{\nabla})\dot{\vec{x}} = -\frac{\vec{\nabla}\Psi}{a^2} + \kappa(t)\dot{\vec{x}}. \tag{42}$$

$$\Rightarrow \ddot{\delta} + (2H - (1+n)\kappa)\dot{\delta} = 4\pi G\varrho_b\delta + 2n\kappa(H-\kappa)\delta. \tag{43}$$

The above Equation (43), which is the final result of [3], reduces to the standard equation when κ approaches 0. The simplifying assumption in Equation (41), introduces the parameter n that measures the type of the perturbation. The perturbation type number n in our study is related to the degree of the homogeneous polynomial that describes the constant hyper-surfaces of δ. That is, linear perturbations are represented with $\delta = x^i\, a_i$ for constants a_i, while $\delta = x^i\, x^j\, a_{ij}$ will correspond to quadratic polynomials, and so on.

That is, a spherically symmetric perturbation has $n = 2$. As shown in Figure 6, even at relatively low matter densities, perturbations for various values of $n \geq 1$ result in a faster growth of the density fluctuations than in the Einstein–de Sitter model. Strikingly, the overall slope is independent of the choice of recombination epoch $z_{\rm rec}$.

The behavior for different $\Omega_{\rm m}$ is also interesting (see Figure 7); for example, the smaller $\Omega_{\rm m}$ is, the steeper the growth of the density fluctuations is. It is always much steeper than in the Einstein–de Sitter model. For further details, see the discussion by Maeder and Gueorguiev [3].

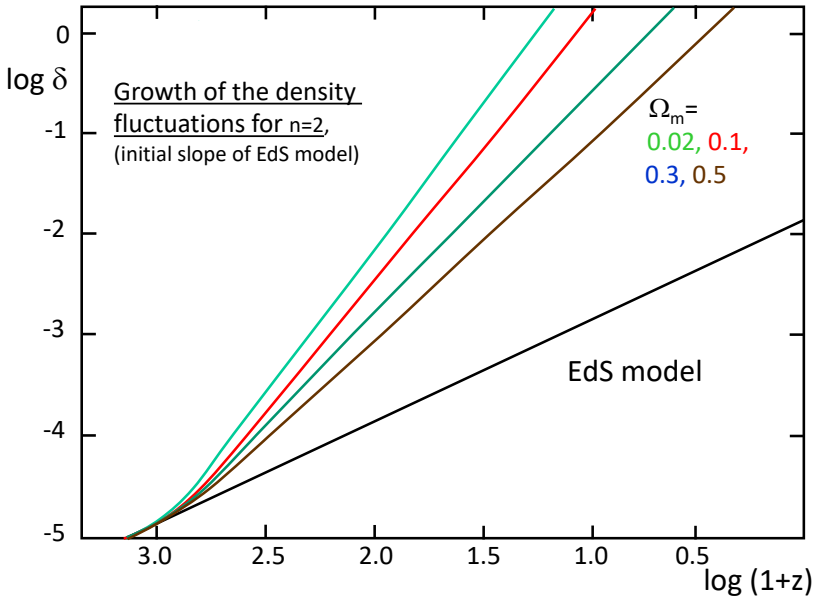


Figure 7. The black curve is the classical growth of the density fluctuations in the Einstein–de Sitter model. The other four curves illustrate the growth of δ for the density profile with $n = 2$ in the scale-invariant theory. There are four different values of the density parameter $\Omega_{\rm m}$. An initial value $\delta = 10^{-5}$ at $z = 1376$ has been taken for all models, the initial derivative $\dot{\delta}$ is taken equal to that of the EdS model. After a short evolution with a slope close to the initial one, all solutions indicate a much faster growth of the density fluctuations, reaching the non-linear regime between about $z+1 = 2.7$ and $z = 18$. Note that $\Omega_{\rm m} = 0.3$ is the dark green curve. Figure reprinted with permission from Maeder and Gueorguiev [3], Copyright 2019 Elsevier.

Over recent years, highly redshifted galaxies have been found, in particular with the observational data from JWST, which suggests very early times of galaxy formation [54]. We point out, as shown by Figure 6, that very early galaxy formation is a process currently expected in the context of the SIV theory.

3.7. Big Bang Nucleosynthesis within the SIV Paradigm [8]

The SIV paradigm has been recently applied to the Big Bang Nucleosynthesis using the known analytic expressions for the expansion factor $a(t)$ and the plasma temperature T as functions of the SIV time τ since the Big Bang, when $a(\tau = 0) = 0$ [8]. The results have been compared to the standard BBNS, as calculated via the PRIMAT code [55]. Potential SIV-guided deviations from the local statistical equilibrium were also explored in [8]. Overall, it was found that smaller-than-usual baryon and non-zero dark matter content, by a reduction factor of three to five times, result in compatibility to the standard light elements abundances (Table 2).

Table 2. The observational uncertainties are 1.6% for Y_P, 1.2% for D/H, 18% for T/H, and 19% for Li/H. FRF is the forwards rescale factor for all reactions, while m$\check{\mathrm{T}}$ and Q/$\check{\mathrm{T}}$ are the corresponding rescale factors in the reverse reaction formula based on the local thermodynamical equilibrium. The SIV λ-dependences are used when these factors are different from 1; that is, in the sixth and ninth columns, where FRF = λ, m$\check{\mathrm{T}}$ = $\lambda^{-1/2}$, and Q/$\check{\mathrm{T}}$ = $\lambda^{+1/2}$. The columns denoted by fit contain the results for perfect fit on Ω_b and Ω_m to ^{4}He and D/H, while fit* is the best possible fit on Ω_b and Ω_m to the ^{4}He and D/H observations for the model considered, as indicated in the columns four and seven. The last three columns are usual PRIMAT runs with modified $a(T)$ such that $\bar{a}/\lambda = a_{SIV}/S^{1/3}$, where $\bar{a}$ is the PRIMAT's $a(T)$ for the decoupled neutrinos case. Column seven is actually $a_{SIV}/S^{1/3}$, but it is denoted by $\bar{a}/\lambda$ to remind us about the relationship $a' = a\lambda$; the run is based on Ω_b and Ω_m from column five. The smaller values of η_{10} are due to smaller $h^2\Omega_b$, as seen by noting that η_{10}/Ω_b is always ≈ 1.25. Table originally presented in [8].

Element	**Obs.**	**PRMT**	a_{SIV}	**fit**	**fit***	$\bar{a}/\lambda$	**fit***	**fit**
H	0.755	0.753	0.805	0.755	0.849	0.75	0.753	0.755
$Y_P = 4Y_\mathrm{He}$	0.245	0.247	0.195	0.245	0.151	0.25	0.247	0.245
D/H $\times 10^5$	2.53	2.43	0.743	2.52	2.52	1.49	2.52	2.53
^{3}He/H $\times 10^5$	1.1	1.04	0.745	1.05	0.825	0.884	1.05	1.04
^{7}Li/H $\times 10^{10}$	1.58	5.56	11.9	5.24	6.97	9.65	5.31	5.42
N_eff	3.01	3.01	3.01	3.01	3.01	3.01	3.01	3.01
η_{10}	6.09	6.14	6.14	1.99	0.77	1.99	5.57	5.56
FRF	1	1	1	1	1.63	1	1	1.02
m$\check{\mathrm{T}}$	1	1	1	1	0.78	1	1	0.99
Q/$\check{\mathrm{T}}$	1	1	1	1	1.28	1	1	1.01
Ω_b [%]	4.9	4.9	4.9	1.6	0.6	1.6	4.4	4.4
Ω_m [%]	31	31	31	5.9	23	5.9	86	95
$\sqrt{\chi^2_\epsilon}$	N/A	6.84	34.9	6.11	14.8	21.9	6.2	6.4

The SIV analytic expressions for $a(T)$ and $\tau(T)$ were utilized to study the BBNS within the SIV paradigm [8,33]. The functional behavior is very similar to the standard model within PRIMAT except during the very early universe, where electron–positron annihilation and neutrino processes affect the $a(T)$ function (see Table I and Figure 2 in [8]). The distortion due to these effects encoded in the function $S(T)$ could be incorporated by considering the SIV paradigm as a background state of the universe where these processes could take place. It has been demonstrated that the incorporation of the $S(T)$ within the SIV paradigm results in a compatible outcome with the standard BBNS; see the last two columns of Table 2; furthermore, if one is to fit the observational data, the result is $\lambda \approx 1$ for the SIV parameter λ (see last column of Table 2 with $\lambda = \mathrm{FRF} \approx 1$). However, a pure SIV treatment (the middle three columns) results in $\Omega_b \approx 1\%$ and less total matter, either around $\Omega_\mathrm{m} \approx 23\%$ when all the λ-scaling connections are utilized (see Table 2 column 6), or around $\Omega_\mathrm{m} \approx 6\%$ without any λ-scaling factors (see column 5). The need to have λ close to 1 is not an indicator of dark matter content but indicates the goodness of the standard PRIMAT results that allow only for λ close to 1 as an augmentation, as such, this leads to a slight but important improvement in D/H, as seen when comparing columns three with eight and nine.

The SIV paradigm suggests specific modifications to the reaction rates, as well as the functional temperature dependences of these rates, that need to be implemented to obtain consistency between the EGR frame and the WIG (SIV) frame. In particular, the non-in-scalar factor T^{β} in the reverse reactions rates may be affected the most due, to the SIV effects. As shown in [8], the specific dependences studied, within the assumptions made within the SIV model, resulted in three times less baryon matter, usually around $\Omega_b \approx 1.6\%$ and less total matter, around $\Omega_{\rm m} \approx 6\%$. The lower baryon matter content also leads to a lower photon-to-baryon ratio $\eta_{10} \approx 2$ within the SIV, which is three tines less that the standard value of $\eta_{10} = 6.09$. As shown in [8], the overall results indicated insensitivity to the specific λ-scaling dependence of the m$\check{\rm T}$-factor in the reverse reaction expressions within T^{β} terms. Thus, one may have to further explore the SIV-guided λ-scaling relations, as done for the last column in Table 2; however, this would require the utilization of the numerical methods used by PRIMAT and, as such, will take us away from the SIV-analytic expressions explored that provided a simple model for understanding the BBNS within the SIV paradigm. Furthermore, it will take us further away from the accepted local statistical equilibrium and may require the application of the reparametrization paradigm that seems to result in SIV-like equations but does not impose a specific form for λ [10]. Thus, at this point, the SIV theory is still a viable alternative model for cosmology.

To sum up, the SIV paradigm provides an alternative model for cosmology that suggests a reduction in baryon and non-zero dark matter content, leading to compatible predictions for the light element abundances in the early universe (see Table 2). It also offers a potential mechanism for understanding deviations from the local statistical equilibrium due to possible differences in scaling for matter energy and radiation energy, (m$\check{\rm T}$ and Q/$\check{\rm T}$). Furthermore, the SIV paradigm has been applied to the Big Bang Nucleosynthesis using known analytic expressions for the expansion factor and plasma temperature, resulting in predictions that differ from those of standard cosmological models about the baryon and the dark matter content (see Table 2). In particular, since the $t_{\rm in}$ is related to the total matter content $\Omega_{\rm m}$, and, as such, enters most of the SIV analytic expressions, this makes possible to assess the dark matter content during the SIV BBNS, unlike the standard BBNS treatment. That is, the SIV theory also predicts a reduction in baryon and non-zero dark matter content, leading to compatible predictions for the light element abundances; see Table 2.

3.8. SIV and the Inflation of the Early Universe [5]

Another important result within the SIV paradigm is the presence of an inflationary stage at the very early universe $t \approx t_{\rm in} \ll t_0 = 1$, with a natural exit from inflation in a later time $t_{\rm exit}$, with a value related to the parameters of the inflationary potential [5]. The main steps towards these results are outlined below.

By reviewing the general scale-invariant cosmological Equation (9), we can derive an expression for the vacuum energy density that connects the cosmological constant Λ with the energy density expressed in terms of $\kappa = -\dot{\lambda}/\lambda$. That is, by using the SIV result (14), the vacuum energy density ρ, with $C = 3/(4\pi G)$, is then

$$\rho = \frac{\Lambda}{8\pi G} = \lambda^2 \rho' = \lambda^2 \frac{\Lambda_E}{8\pi G} = \frac{3}{8\pi G}\frac{\dot{\lambda}^2}{\lambda^2} = \frac{C}{2}\dot{\psi}^2 . \tag{44}$$

This provides a natural connection to inflation within the SIV via $\dot{\psi} = -\dot{\lambda}/\lambda$ or $\psi \propto \ln(t)$. The equations for the energy density, pressure, and Weinberg's condition for inflation within the standard model for inflation by Guth [56], Linde [57,58], and Weinberg [59] are

$$\left.\begin{matrix}\rho \\ p\end{matrix}\right\} = \frac{1}{2}\dot{\varphi}^2 \pm V(\varphi), \; \mid \dot{H}_{\rm infl} \mid \ll H^2_{\rm infl} . \tag{45}$$

If we make the identification between the standard model for inflation above with the fields present within the SIV (using $C = 3/(4\pi G)$),

$$\dot{\psi} = -\dot{\lambda}/\lambda, \quad \varphi \leftrightarrow \sqrt{C}\,\psi, \quad V \leftrightarrow CU(\psi), \quad U(\psi) \;=\; g\, e^{\mu\,\psi}\,. \tag{46}$$

Here, $U(\psi)$ is the inflation potential with strength g and field "coupling" μ. One can evaluate Weinberg's condition for inflation (45) within the SIV framework [5], and the result is

$$\frac{\mid \dot{H}_{\rm infl} \mid}{H^2_{\rm infl}} \;=\; \frac{3\,(\mu+1)}{g\,(\mu+2)}\, t^{-\mu-2} \ll 1 \;\text{ for }\; \mu < -2, \text{ and } \; t \ll t_0 = 1. \tag{47}$$

When Weinberg's condition for inflation (45) is not satisfied anymore, one can see that there is a graceful exit from inflation at the later time:

$$t_{\rm exit} \approx \sqrt[n]{\frac{n\,g}{3(n+1)}} \qquad \text{with} \qquad n = -\mu - 2 > 0. \tag{48}$$

The derivation of Equation (47) starts with the use of the scale-invariant energy conservation equation within the SIV [2,5]:

$$\frac{d(\varrho a^3)}{da} + 3\,pa^2 + (\varrho + 3\,p)\frac{a^3}{\lambda}\frac{d\lambda}{da} = 0\,, \tag{49}$$

which has the following equivalent form:

$$\dot{\varrho} + 3\,\frac{\dot{a}}{a}\,(\varrho + p) + \frac{\dot{\lambda}}{\lambda}\,(\varrho + 3p) \;=\; 0\,. \tag{50}$$

By substituting the expressions for ρ and p from (45) along with the SIV identification (46) within the SIV expression (50), one obtains a modified form of the Klein–Gordon equation, which could be non-linear when using non-linear potential $U(\psi)$ as in (46):

$$\ddot{\psi} + U' \,+ 3H_{\rm infl}\,\dot{\psi} - 2\,(\dot{\psi}^2 - U) \;=\; 0\,. \tag{51}$$

The above Equation (51) can be used to evaluate the time derivative of the Hubble parameter. The process utilizes (14); that is, $\lambda = t_0/t$, $\dot{\psi} = -\dot{\lambda}/\lambda = 1/t \;\Rightarrow \ddot{\psi} = -\dot{\psi}^2$, along with $\psi = \ln(t) + const$ and $U(\psi) \;=\; g\, e^{\mu\,\psi} = g t^{\mu}$ when the normalization of the field ψ is chosen, so that $\psi(t_0) = \ln(t_0) = 0$ for $t_0 = 1$ at the current epoch. The final result is

$$H_{\rm infl} = \dot{\psi} - \frac{2\,U}{3\,\dot{\psi}} - \frac{U'}{3\,\dot{\psi}} \;\;=\;\; \frac{1}{t} - \frac{(2+\mu)\,g}{3}\,t^{\mu+1}\,, \tag{52}$$

$$\dot{H}_{\rm infl} = -\dot{\psi}^2 - \frac{2U}{3} - U' - \frac{U''}{3} \;\;=\;\; -\frac{1}{t^2} - \frac{(\mu+2)(\mu+1)\,g}{3}t^{\mu}\,. \tag{53}$$

For $\mu < -2$, the t^{μ} terms above are dominant; thus, the critical ratio (45) for the occurrence of inflation near $t \approx t_{\rm in}$ is then

$$\frac{\mid \dot{H}_{\rm infl} \mid}{H^2_{\rm infl}} \;=\; \frac{3\,(\mu+1)}{g\,(\mu+2)}\, t^{-\mu-2}\,.$$

Equations (15) and (44), derived from the field equations of the SIV, indicate that both the energy density ϱ and the cosmological constant Λ within the SIV exhibit a $1/t^2$ behavior. This implies an enormous increase in the vacuum energy density and the cosmological constant Λ within the SIV as we approach the Big Bang moment. For instance, characterized by the dominance of quantum effects, at the Planck time $t_{\rm Pl} = 5.39 \cdot 10^{-44}$ s, the cosmological constant would be approximately $\left(\frac{4.355 \cdot 10^{17}}{5.39 \cdot 10^{-44}}\right)^2 = 6.4 \cdot 10^{121}$ times larger than its present-day value based on the current age of $\tau_0 \;=\; 13.7$ Gyr $\;=\; 4.323 \cdot 10^{17}$ s.

This behavior may offer a potential resolution to the cosmological constant problem by considering Planck-seed universes and derivable universes as distinct phases of the same universe rather than disconnected entities [31]. Therefore, the remarkably small value of the Einstein cosmological constant Λ_E is inherently linked to the current age of the universe, assuming that $\lambda_0 = 1$ for the usual SIV choice of units. This line of reasoning is further supported by the solution (15) for (14) that implies $\Lambda_E = 3/\tau_0^2 \approx 1.6 \times 10^{-35}$ s^{-2}, in agreement with modern observations.

In short, the SIV paradigm provides an alternative model for cosmology that includes a natural exit from inflation in the early universe (see Equation (48)). This is supported by the presence of an inflationary stage at the very early universe when $t_{\rm in} < t < t_{\rm exit}$, along with the connection between the scale factor and the conventional inflation field (46).

4. Conclusions and Outlook

The SIV hypothesis is a relatively new theory, and it is still under development. However, the results of the tests that have been conducted so far are promising. If the SIV hypothesis is correct, it could provide a new and important understanding of the universe.

Based on the previous sections on various comparisons, one can conclude that the *SIV cosmology is a viable alternative to* ΛCDM. In particular, *the cosmological constant disappears* within the SIV gauge (16). As emphasized in the discussion presented in Section 3.1 from [2], there are diminishing differences in the values of the scale factor $a(t)$ within ΛCDM and the SIV at higher densities. The SIV also shows consistency for H_0 and the age of the universe, and the m-z diagram is well satisfied (see Maeder and Gueorguiev [6] for details).

Furthermore, *the SIV provides the correct RAR for dwarf spheroidals* (Figure 5), while this is more difficult for MOND, and even more difficult for dark matter, which cannot yet account for the phenomenon [4]. However, the observations still have some degree of uncertainty. What is clear, is that, as in other cases, within the SIV, dark matter is not needed.

Thus, as emphasized in Gueorguiev and Maeder [1]: "it seems that *within the SIV, dark matter is not needed to seed the growth of structure* in the universe". As depicted in Figure 6, there is a sufficiently rapid growth of density fluctuations. A more detailed discussion of this observation is given in [3]. Therefore, key aspects or observations that distinguish the SIV from the standard cosmological model based on the usual cosmological tests are the relations m-M vs. z, but the differences are very small, and there is no hope to solve the question rapidly. For low $\Omega_{\rm m}$, the values are a bit larger and could allow some differentiation. The redshift drifts (see Figure 4) are like the most powerful tests, but we have to wait for a decade or two. For now, the main effects concern the growth of density fluctuations (see Figure 6), the rotation curves of galaxies, which are well reproduced within MOND, which has been shown to be a peculiar case of the SIV. This connection of SIV-derived MOND a_0, which depends on $\Omega_{\rm m}$ and z within the SIV, has prompted researchers to explore the z-dependence of the a_0 [41].

In our study, on inflation within the SIV cosmology, we identified a connection between λ and its rate of change, $\dot{\psi} = -\dot{\lambda}/\lambda$ (46), to the conventional inflation field φ, that is, $\psi \to \varphi$. As seen from (47), *inflation of the very, very early universe*, $\tau \approx 0$ $(t \approx t_{in} \ll 1)$, *is natural, and SIV predicts a graceful exit from inflation* (see (48))!

Our latest study on the primordial nucleosynthesis within the SIV [8] has shown that smaller-than-usual baryon and non-zero dark matter content, by a reduction factor of three to five times, result in compatibility to the standard light elements abundances (Table 2).

Some of the obvious future research directions are related to primordial nucleosynthesis, where preliminary results show a satisfactory comparison between the SIV and observations [8,33]. Further investigations of potential SIV-guided deviations from the local statistical equilibrium should be studied, since this may lead to mechanisms for understanding the matter–anti-matter asymmetry. The recent success of the R-MOND in the description of the CMB [38], after the initial hope and concerns [60], is very stimulating; it suggests that a generally covariant theory that has the correct Newtonian limit is likely to describe the CMB. Since the SIV is generally covariant and has the correct limits, it demands

the testing of the SIV cosmology as well against the MOND and ΛCDM successes in the description of the CMB, the Baryonic Acoustic Oscillations, etc.

Another area of research is to better understand the physical meaning of λ. As it was pointed out in Section 1.2, a general conformal factor seems to be linked to Jordan–Brans–Dicke's scalar-tensor theory, resulting in a varying Newton's constant G that has not yet been detected. Introducing a spatially dependent conformal factor allows for localized field excitations that could be interpreted as fundamental scalar particles. While the Higgs boson is an example of such a particle, a link to Jordan–Brans–Dicke's scalar-tensor theory appears improbable. Conversely, assuming spatial isotropy and homogeneity forces the coupling constant λ to be time-dependent, which differs significantly from the behavior of known fundamental fields. Thus, the specific time dependence for $\lambda(t) = t_0/t$ and the absence of spatial dependence are important hallmarks of the SIV paradigm. As such, they have to be maintained and appropriately derived from the basic tenets of the SIV theory towards its future applications.

Furthermore, some less obvious directions are the solar system exploration due to the high-accuracy data there, or exploring in more detail the connection to the reparametrization invariance. In particular, it is known from Gueorguiev and Maeder [10] that un-proper time parametrization leads to equations of motion (5) corresponding with the weak-field SIV limit (29).

Author Contributions: Writing—original draft V.G.G., conceptualization—both authors; formal analysis—both authors; investigation—both authors; methodology—both authors; validation—both authors; writing—review and editing—both authors; both co-authors have been actively involved in the writing of the paper and its draft versions. All authors have read and agreed to the published version of the manuscript.

Funding: This research received no external funding.

Data Availability Statement: No new data were created or analyzed in this study.

Acknowledgments: A.M. expresses their gratitude to their wife for her patience and support. V.G. is extremely grateful to their wife and daughters for their understanding and family support during the various stages of the research presented. This research did not receive any specific grant from funding agencies in the public, commercial, or not-for-profit sectors.

Conflicts of Interest: The authors declare no conflicts of interest.

Appendix A. On the Error by Banik and Kroupa (2020) Concerning the Lunar Motion in the Scale-Invariant Theory

The scale-invariant theory has been criticized by Banik, I., Kroupa, P. (2020), MNRAS 497, L62 (BK20), concerning lunar motion. They claim that the observed orbital angular velocity Ω of the Moon is incompatible with the interpretation of the lunar recession in the scale-invariant theory (SIV) by Maeder and Gueorguiev [4]. In fact, their argument is vitiated at the basis since, in being willing to apply Kepler's third law and the scale-invariant effects, they use a strange mixture of classical and scale-invariant expressions, which is totally inconsistent. They write the following expression for the relative variations of the angular velocity:

$$\frac{\dot{\Omega}}{\Omega} = -\frac{\dot{r}_{\mathrm{SIV}} + (3/2)\dot{r}_{\mathrm{tide}}}{r}. \tag{A1}$$

Interestingly enough, the general field equation in the scale-invariant context has been demonstrated from an action principle by Maeder and Gueorguiev [9], and as a consequence, the modified Newton's Law, which results in the weak-field low-velocity approximation, contains an additional acceleration term. However, Kepler's third law re-

mains unmodified in the scale-invariant context [9]. This implies that the correct expression for the relative variations of the angular velocity in the SIV theory is

$$\frac{\dot{\Omega}}{\Omega} = \frac{\dot{M}}{2M} - \frac{3}{2}\left(\frac{\dot{r}}{r}\right)_{\text{eff}} \tag{A2}$$

since there is small secular change of the inertial (and gravitational mass). Without this small effect, the expression would be the same as the classical one.

The effective changes of the Moon's orbital radius $\left(\frac{\dot{r}}{r}\right)_{\text{eff}}$ is the above expression of $dR/d\tau$, see Equation (48) in [7], which contains all the intervening effects: the Moon–Earth tides, the change of the moment of inertia of the Earth, and the global expansion.

We have seen that the calculated resulting effect in the SIV is remarkably consistent with the Moon's observed recession for a value of Ω_{m}, which is also consistent with little or no dark matter. It should also be pointed out that the contribution to the Moon–Earth tides used in the above calculation only rests on the slowing down of the Earth rotation based on the data by Stephenson et al. [47,49], who analyzed the ancient lunar and solar eclipses since the time of the Babylonians, which imply the presence of an additional effect in the lunar recession [53].

Now, the expression of $\left(\frac{\dot{\Omega}}{\Omega}\right)$ can be calculated using the indicated values of $\left(\frac{\dot{r}}{r}\right)_{\text{eff}}$. For $\frac{\dot{M}}{2M}$, we use the appropriate expression of $\frac{\dot{M}}{M} = \frac{(1-\Omega_{\text{m}}^{1/3})}{\tau_0}$, where τ_0 is the present age of the universe (13.8 Gyr). The resulting values of $\left(\frac{\dot{\Omega}}{\Omega}\right)$ are are in the range of

$$\left(\frac{\dot{\Omega}}{\Omega}\right) = (1.24 \div 1.38) \cdot 10^{-11}\,\text{s}, \quad \text{for } \Omega_{\text{m}} = 0.30 \div 0.01, \tag{A3}$$

compared to a value of $1.42 \cdot 10^{-11}$ s, corresponding to the observed ratio. This is not perfect, but it is a most remarkable agreement if we think that this last value is the result of the observed slowing down of the Earth since the Babylonians and involves the age of the universe along with Ω_{m}. Thus, the claim that the scale-invariant results deviate by more than 200 σ from the observations is essentially due to the wrong expression (A1), imagined and used by Banik and Kroupa. On the contrary, such an accurate value of $\left(\frac{\dot{\Omega}}{\Omega}\right)$ derived from the empirical slowing down of the Earth is remarkable in view of the many uncertainties in the physics of the Earth–Moon system.

Finally, Banik and Kroupa also comment on the problem that may be set by a mass variation in the stellar evolution. This problem has been well treated by Maeder (1977, *Astronomy and Astrophysics*, 56, 359), who showed that when the product GM varies like t, the evolutionary tracks are very similar to the standard ones. In particular, they give the right solar luminosity for an age of 4.57 Gyr. Moreover, the tracks and isochrones of other masses (even for old stars) are undiscernable from the standard ones. A careful comparison was made in the case of the well-studied old cluster M67, which showed perfect agreement. Moreover, the neutrino flux was reduced by a factor of two. New models are also presently foreseen with colleagues at the Geneva Observatory.

References

1. Gueorguiev, V.G.; Maeder, A. The Scale Invariant Vacuum Paradigm: Main Results and Current Progress. *Universe* **2022**, *8*, 213. [CrossRef]
2. Maeder, A. An Alternative to the ΛCDM Model: The Case of Scale Invariance. *Apj* **2017**, *834*, 194, [CrossRef]
3. Maeder, A.; Gueorguiev, V.G. The growth of the density fluctuations in the scale-invariant vacuum theory. *Phys. Dark Universe* **2019**, *25*, 100315. [CrossRef]
4. Maeder, A.; Gueorguiev, V.G. Scale-invariant dynamics of galaxies, MOND, dark matter, and the dwarf spheroidals. *Mon. Not. R. Astron. Soc.* **2020**, *492*, 2698–2708. [CrossRef]
5. Maeder, A.; Gueorguiev, V.G. Scale invariance, horizons, and inflation. *Mon. Not. R. Astron. Soc.* **2021**, *504*, 4005–4014. [CrossRef]
6. Maeder, A.; Gueorguiev, V.G. The Scale-Invariant Vacuum (SIV) Theory: A Possible Origin of Dark Matter and Dark Energy. *Universe* **2020**, *6*, 46. [CrossRef]

7. Maeder, A.; Gueorguiev, V. Local Dynamical Effects of Scale Invariance: The Lunar Recession. *arXiv* **2022**, arXiv:2204.13560. [CrossRef]
8. Gueorguiev, V.G.; Maeder, A. Big-Bang Nucleosynthesis within the Scale Invariant Vacuum Paradigm. *arXiv* **2023**, arXiv:2307.04269. [CrossRef]
9. Maeder, A.; Gueorguiev, V.G. Action Principle for Scale Invariance and Applications (Part I). *Symmetry* **2023**, *15*, 1966. [CrossRef]
10. Gueorguiev, V.G.; Maeder, A. Geometric Justification of the Fundamental Interaction Fields for the Classical Long-Range Forces. *Symmetry* **2021**, *13*, 379. [CrossRef]
11. Weyl, H. *Raum, Zeit, Materie. Vorlesungen über Allgemeine Relativitätstheorie*; Springer: Berlin/Heidelberg, Germany, 1970.
12. Brans, C.H. Jordan-Brans-Dicke Theory. *Scholarpedia* **2014**, *9*, 31358. [CrossRef]
13. Faraoni, V.; Gunzig, E.; Nardone, P. Conformal transformations in classical gravitational theories and in cosmology. *Fund. Cosmic Phys.* **1999**, *20*, 121–175. [CrossRef]
14. Behnke, D.; Blaschke, D.B.; Pervushin, V.N.; Proskurin, D. Description of supernova data in conformal cosmology without cosmological constant. *Phys. Lett. B* **2002**, *530*, 20–26. [CrossRef]
15. Jackiw, R.; Pi, S.Y. Fake conformal symmetry in conformal cosmological models. *Phys. Rev. D* **2015**, *91*, 067501. [CrossRef]
16. Tsamis, N.C.; Woodard, R.P. Gauge problems with the equations of motion. *Class. Quantum Gravity* **1985**, *2*, 841–867. [CrossRef]
17. Christodoulou, D.M.; Kazanas, D. Varying-G gravity: Physical properties, asymptotic regimes, and Green's functions, an event horizon, the vacuum energy density, and the external pressure that modifies Jeans stability. *Mon. Not. R. Astron. Soc.* **2023**, *519*, 1277–1292. [CrossRef]
18. Xue, C.; Liu, J.P.; Li, Q.; Wu, J.F.; Yang, S.Q.; Liu, Q.; Shao, C.G.; Tu, L.C.; Hu, Z.K.; Luo, J. Precision measurement of the Newtonian gravitational constant. *Natl. Sci. Rev.* **2020**, *7*, 1803–1817. [CrossRef] [PubMed]
19. Dirac, P.A.M. Long Range Forces and Broken Symmetries. *Proc. R. Soc. Lond. Ser. A* **1973**, *333*, 403–418. [CrossRef]
20. Canuto, V.; Adams, P.J.; Hsieh, S.H.; Tsiang, E. Scale-covariant theory of gravitation and astrophysical applications. *Phys. Rev. D* **1977**, *16*, 1643–1663. [CrossRef]
21. Gueorguiev, V.G.; Maeder, A. Reparametrization Invariance and Some of the Key Properties of Physical Systems. *Symmetry* **2021**, *13*, 522. [CrossRef]
22. Wheeler, J.T. Weyl geometry. *Gen. Relativ. Gravit.* **2018**, *50*, 80. [CrossRef]
23. Zakharov, A.F.; Pervushin, V.N. Conformal Cosmological Model Parameters with Distant SNe ia Data: "gold" and "silver". *Int. J. Mod. Phys. D* **2010**, *19*, 1875–1887. [CrossRef]
24. Pervushin, V.N.; Arbuzov, A.B.; Zakharov, A.F. Estimation of conformal cosmological model parameters with SDSS and SNLS supernova samples. *Phys. Part. Nucl. Lett.* **2017**, *14*, 368–370. [CrossRef]
25. Lee, S. Constraints on the time variation of the speed of light using Pantheon dataset. *arXiv* **2021**, arXiv:2101.09862. [CrossRef]
26. Gupta, R.P. Testing CCC+TL Cosmology with Observed Baryon Acoustic Oscillation Features. *Astrophys. J.* **2024**, *964*, 55. [CrossRef]
27. Newell, D.B.; Tiesinga, E. The international system of units (SI). *NIST Spec. Publ.* **2019**, *330*, 1–138.
28. Maeder, A.; Bouvier, P. Scale invariance, metrical connection and the motions of astronomical bodies. *Astron. Astrophys.* **1979**, *73*, 82–89.
29. Bouvier, P.; Maeder, A. Consistency of Weyl's Geometry as a Framework for Gravitation. *Astrophys. Space Sci.* **1978**, *54*, 497–508. [CrossRef]
30. Dirac, P.A.M. Cosmological Models and the Large Numbers Hypothesis. *Proc. R. Soc. Lond. Ser. A* **1974**, *338*, 439–446. [CrossRef]
31. Gueorguiev, V.G.; Maeder, A. Revisiting the Cosmological Constant Problem within Quantum Cosmology. *Universe* **2020**, *6*, 108. [CrossRef]
32. Jesus, J.F. Exact Solution for Flat Scale-Invariant Cosmology. *arXiv* **2017**, arXiv:1712.00697. [CrossRef]
33. Maeder, A. Evolution of the early Universe in the scale invariant theory. *arXiv* **2019**, arXiv:1902.10115. [CrossRef]
34. Maeder, A. MOND as a peculiar case of the SIV theory. *Mon. Not. R. Astron. Soc.* **2023**, *520*, 1447–1455. [CrossRef]
35. Frieman, J.A.; Turner, M.S.; Huterer, D. Dark energy and the accelerating universe. *Annu. Rev. Astron. Astrophys.* **2008**, *46*, 385–432. [CrossRef]
36. Lusso, E.; Piedipalumbo, E.; Risaliti, G.; Paolillo, M.; Bisogni, S.; Nardini, E.; Amati, L. Tension with the flat ΛCDM model from a high-redshift Hubble diagram of supernovae, quasars, and gamma-ray bursts. *Astron. Astrophys.* **2019**, *628*, L4. [CrossRef]
37. Liske, J.; Grazian, A.; Vanzella, E.; Dessauges, M.; Viel, M.; Pasquini, L.; Haehnelt, M.; Cristiani, S.; Pepe, F.; Avila, G.; et al. Cosmic dynamics in the era of Extremely Large Telescopes. *Mon. Not. R. Astron. Soc.* **2008**, *386*, 1192–1218. [CrossRef]
38. Skordis, C.; Złośnik, T. New Relativistic Theory for Modified Newtonian Dynamics. *Phys. Rev. Lett.* **2021**, *127*, 161302. [CrossRef]
39. Clifton, T.; Ferreira, P.G.; Padilla, A.; Skordis, C. Modified gravity and cosmology. *Phys. Rep.* **2012**, *513*, 1–189. [CrossRef]
40. Capozziello, S.; de Laurentis, M. Extended Theories of Gravity. *Phys. Rep.* **2011**, *509*, 167–321. [CrossRef]
41. Del Popolo, A.; Chan, M.H. On the time dependency of a_0. *Phys. Dark Universe* **2024**, *43*, 101415. [CrossRef]
42. Milgrom, M. Cosmological variation of the MOND constant: Secular effects on galactic systems. *Phys. Rev. D* **2015**, *91*, 044009. [CrossRef]
43. Feynman, R.P. *Feynman Lectures on Physics*; Addison-Wesley: Reading, MA, USA, 1963; Volume 1.
44. Williams, J.G.; Boggs, D.H.; Ratcliff, J.T. Lunar Tidal Recession. In Proceedings of the 47th Annual Lunar and Planetary Science Conference, Woodlands, TX, USA, 21–25 March 2016; p. 1096.

45. Williams, J.G.; Boggs, D.H. Secular tidal changes in lunar orbit and Earth rotation. *Celest. Mech. Dyn. Astron.* **2016**, *126*, 89–129. [CrossRef]
46. Christodoulidis, D.C.; Smith, D.E.; Williamson, R.G.; Klosko, S.M. Observed Tidal Braking in the Earth/moon/sun System. *J. Geophys. Res.* **1988**, *93*, 6216–6236. [CrossRef]
47. Stephenson, F.R.; Morrison, L.V.; Hohenkerk, C.Y. Measurement of the Earth's rotation: 720 BC to AD 2015. *Proc. R. Soc. Lond. Ser. A* **2016**, *472*, 20160404. [CrossRef]
48. Deines, S.D.; Williams, C.A. Earth's Rotational Deceleration: Determination of Tidal Friction Independent of Timescales. *Astron. J.* **2016**, *151*, 103. [CrossRef]
49. Stephenson, F.R.; Morrison, L.V.; Hohenkerk, C.Y. Eclipses and the Earth's Rotation. In *Proceedings of the IAU General Assembly*; Cambridge University Press: Cambridge, UK, 2020; pp. 160–162. [CrossRef]
50. McCarthy, D.D.; Babcock, A.K. The length of day since 1656. *Phys. Earth Planet. Inter.* **1986**, *44*, 281–292. [CrossRef]
51. Sidorenkov, N.S. The effect of the El Nino Southern oscillation on the excitation of the Chandler motion of the Earth's pole. *Astron. Rep.* **1997**, *41*, 705–708.
52. Williams, J.G. Contribution to the Earth's Obliquity Rate, Precession, and Nutation. *Astron. J.* **1994**, *108*, 711. [CrossRef]
53. Maeder, A.M.; Gueorguiev, V.G. On the relation of the lunar recession and the length-of-the-day. *Astrophys. Space Sci.* **2021**, *366*, 101. [CrossRef]
54. Bunker, A.J.; Saxena, A.; Cameron, A.J.; Willott, C.J.; Curtis-Lake, E.; Jakobsen, P.; Carniani, S.; Smit, R.; Maiolino, R.; Witstok, J.; et al. JADES NIRSpec Spectroscopy of GN-z11: Lyman-α emission and possible enhanced nitrogen abundance in a z = 10.60 luminous galaxy. *Astron. Astrophys.* **2023**, *677*, A88. [CrossRef]
55. Pitrou, C.; Coc, A.; Uzan, J.P.; Vangioni, E. Precision big bang nucleosynthesis with improved Helium-4 predictions. *Phys. Rep.* **2018**, *754*, 1–66. [CrossRef]
56. Guth, A.H. Inflationary universe: A possible solution to the horizon and flatness problems. *Phys. Rev. D* **1981**, *23*, 347–356. [CrossRef]
57. Linde, A. Lectures on inflationary cosmology. *arXiv* **1995**, arXiv:hep-th/9410082. [CrossRef]
58. Linde, A. Particle Physics and Inflationary Cosmology. *arXiv* **2005**, arXiv:hep-th/0503203. [CrossRef]
59. Weinberg, S. *Cosmology*; Oxford University Press: Oxford, UK, 2008.
60. Skordis, C.; Mota, D.F.; Ferreira, P.G.; Bœhm, C. Large Scale Structure in Bekenstein's Theory of Relativistic Modified Newtonian Dynamics. *Phys. Rev. Lett.* **2006**, *96*, 011301. [CrossRef]

Disclaimer/Publisher's Note: The statements, opinions and data contained in all publications are solely those of the individual author(s) and contributor(s) and not of MDPI and/or the editor(s). MDPI and/or the editor(s) disclaim responsibility for any injury to people or property resulting from any ideas, methods, instructions or products referred to in the content.